

# Modeling and evaluating nodal resilience of multi-energy systems under windstorms

Minglei Bao<sup>a</sup>, Yi Ding<sup>a,\*</sup>, Maosheng Sang<sup>a</sup>, Daqing Li<sup>b</sup>, Changzheng Shao<sup>a</sup>, Jinyue Yan<sup>c,d</sup>

<sup>a</sup> College of Electrical Engineering, Zhejiang University, Hangzhou 310058, China

<sup>b</sup> School of Reliability and Systems Engineering, Beihang University, Beijing 100191, China

<sup>c</sup> School of Business, Society and Energy, Mälardalen University, Västerås, Sweden

<sup>d</sup> School of Chemical Science and Engineering, Royal Institute of Technology, Stockholm, Sweden

## HIGHLIGHTS

- A framework is proposed for the resilience analysis of multi-energy systems.
- Nodal metrics are defined to quantify the resilience of multi-energy systems.
- The resilience performance of multi-energy systems can differ in different regions.
- The increase of wind speeds can notably decrease the system resilience indicators.

## ARTICLE INFO

### Keywords:

Multi-energy systems  
Windstorms  
Optimal energy flow model  
Nodal resilience  
Monte-Carlo simulation method

## ABSTRACT

With the growing frequency and extent of extreme weather events, the resilient operation of multi-energy systems (MESs) has drawn attention nowadays. However, there is little study on the methodology with a set of key indicators to quantify the resilience of MESs with the consideration of the impacts of extreme weather. To address the problem, this paper proposes a framework to evaluate the time-dependent resilience of MESs considering energy interactions during extreme weather events, such as windstorms. Firstly, the multi-phase performance curve is utilized to describe the response behavior of MESs at different phases under the impacts of windstorms. Secondly, a service-based optimal energy flow model is developed to minimize the consequences caused by windstorms through the coordination among different energy subsystems. In order to model the chaotic failures and restoration of components, the Monte-Carlo simulation technique is applied. Furthermore, nodal resilience metrics for different energy carriers are proposed to quantify the resilience in MESs. Numerical studies demonstrate the capability of the proposed technique to quantify the resilience of MESs under windstorms. The results show that the resilience performance level of MESs can differ in different regions with the impacts of windstorms. The findings can provide a useful reference for system operators to constitute targeted resilience improvement measures.

## 1. Introduction

The increasing energy crisis and critical environmental issues have restricted the development of low-carbon smart cities [1]. In order to solve these problems, more and more efforts have been paid to the construction of multi-energy systems (MESs) integrated with different energy carriers, including electricity, natural gas and heat, etc. [2] As composite infrastructure systems, the MESs can provide clean, efficient and sustainable energy for the future smart cities through coordination between various energy subsystems [3].

In the past few decades, climate change has increased the frequency and severity of windstorms and hurricanes [4,5]. Considering the effects of severe weather, the resilient operation of MESs can be threatened, which may lead to long-duration interruption of energy supplied to consumers [6]. It is reported that the catastrophic outages in Texas on 1st February 2011 resulted from windstorms [7]. Considering the impacts of unexpected windstorms, several electrical components can be out of service, including substations and electric lines. Due to the electric supply interruptions caused by windstorms, several electric-driven components in the gas system could not maintain the normal

\* Corresponding author.

E-mail address: [yiding@zju.edu.cn](mailto:yiding@zju.edu.cn) (Y. Ding).

<b>Nomenclature</b>	
<i>Abbreviations</i>	
MESs	multi-energy systems
MCS	Monte-Carlo simulation
DERs	distributed energy resources
EH	energy hub
CHP	combined heat and power
EPL	expected performance loss
CR	collapse ratio
RR	recovery ratio
EGSs	electric-driven gas sources
FGSs	fuel-driven gas sources
EELC	expected electric load curtailments
CRE	collapse ratio of electricity
RRE	recovery ratio of electricity
SEL	synthetic energy loss
IES	isolated electric system
<i>Indices</i>	
$i, j$	index of electric nodes
$m, n$	index of gas nodes
$v$	index of wind speed
$t$	index of time
$s, k$	index of FGSs and EGSs
$c$	index of gas compressors
$g$	index of generators
<i>Parameters and sets</i>	
$\mathbf{AV}$	set of available vector for electrical components
$p_{ij}^0$	the failure probability of overhead line $ij$ under good weather conditions
$M, N$	the total number of gas nodes and electric nodes
$L_{ie}^0, L_{ih}^0$	the electricity demand and heat demand of EH in normal condition [MW, MW]
$\eta_e, \eta_h$	the electrical efficiency and thermal efficiency of CHP [-]
$\varphi$	heat pump efficiency [-]
$\psi$	gas gross heating value [MW/m <sup>3</sup> ]
$\eta_g$	the conversion factor of EGSSs [MW/m <sup>3</sup> ]
$D_{iL}^0, D_{mL}^0$	the initial electric load at electric node $i$ and initial gas load at node $m$ [MW, m <sup>3</sup> ]
$M_{mn}$	constant pipeline flow coefficient [(m <sup>3</sup> /bar) <sup>2</sup> ]
$CO$	the total number of compressors
$\Delta t$	the time interval for the resolution of optimal energy flow model [h]
$ST$	the total simulation times of MCS
<i>Variables</i>	
$p_{ij}(v)$	the failure probability of overhead line $ij$ considering the impacts of storms
$a_{ij}^t$	the operation state of transmission line $ij$
$\Delta L_{ie}^t, \Delta L_{ih}^t$	the electric and heat load curtailment of the EH [MW, MW]
$\Delta P_{iL}^t$	the active load curtailment at node $i$ [MW]
$\Delta W_{mL}^t$	the gas load curtailment at node $m$ [m <sup>3</sup> ]
$\alpha_i^t, v_i^t$	the dispatch factor of electricity flow and gas flow in EH [-]
$P_{i,EH}^t, F_{m,EH}^t$	the input electricity flow and gas flow of EH [MW, m <sup>3</sup> ]
$D_{ik}^t$	the power consumption of EGS $k$ [MW]
$\psi_{mk}^t$	the operation state of EGS $k$ [-]
$f_{mn}^t$	the gas flow through pipeline $mn$ [m <sup>3</sup> ]
$\pi_m^t$	gas pressure at node $m$ [bar]
$W_{ms}^t, W_{mk}^t$	the gas production of EGS and FGS at node $m$ [m <sup>3</sup> , m <sup>3</sup> ]
$f_c^t$	the gas flow through compressor $c$ [m <sup>3</sup> ]
$\tau_c^t$	the compression ratio of compressor $c$ [-]
$P_{ig}^t$	active power output of generator $g$ at node $i$ [MW]
$\theta_i^t$	the phase angle of node $i$ [rad]
$S_{ij}^t$	the power flow on transmission line $ij$ [MW]
$Y_{ij}^t$	the element of admittance matrix for power system
$TTR$	the time to repair damaged components [h]
$\xi$	the variation coefficient of resilience metrics [-]

operation. Under these circumstances, more than 4.4 million energy users' energy consumption (i.e. heat, gas and electricity) was greatly affected during the long-duration blackout [7]. Therefore, considering the dramatic consequences of severe weather, the study on the resilience of integrated energy infrastructure systems has drawn more and more attention nowadays.

Resilience is defined as the ability of systems to resist the possible disturbances, recover to normal operation and adapt to future catastrophic events, which has been widely investigated in society, ecology, engineering and economic systems [8,9]. With respect to energy infrastructure systems, the resilience of power system [10,13], gas system [15], and heat system has been studied independently. Several scholars in electrical engineering concepts focused on the resilience modeling and evaluation of power systems using data-based statistical methods [10,11] and simulation techniques [13,14]. Based on the historical outage data, Ref. [10] estimates the effects of tree trimming on power systems resilience under hurricanes using statistical methods. In Ref. [11], the accelerated failure time models are utilized to estimate the resilience of power grids in terms of power outage durations during hurricanes. Regarding simulation techniques, a three-stage framework is proposed in [12] to analyze the time-dependent resilience of power system under hurricane hazards. Ref. [13] presents a methodology for the spatial and regional resilience assessment of power system affected by severe windstorms. In Ref. [14], a simulation framework is proposed to assess the resilience of power transmission grids subject to cascading

failures under high winds and lightning. At the same time, many scholars focused on the resilience assessment of gas system. Ref. [15] presents a performance assessment methodology to evaluate the resilience of natural gas system considering the impacts of the earthquake. It can be concluded that the previous studies are more focused on the resilience assessment of a single energy system without considering the energy interactions. Actually, the dependent and coupling relationship between different energy carriers in the MESs would definitely influence the resilience of the energy systems, which could not be captured and characterized by the technique in previous studies. Hence, a comprehensive framework needs to be developed to evaluate the resilience of MESs with the consideration of the interactions among different energy subsystems.

In order to quantify the resilience performance of energy systems, various indices have been proposed in the previous studies. For example, the resilience is quantified using the area between the real and target performance curves in [10,16,17]. In Ref. [13], power system resilience is measured by the expected energy losses compared to the pre-event states, while Ref. [16] measures the system resilience using the recovery speeds from post-event degraded states to pre-event states. In Refs. [18,19], system resilience is quantified by the area between the real and target performance curves. However, the previous studies usually adopt system-wide indices to represent the resilience performances of MESs without considering the locational difference of resilience. Due to the limited transmission capacity and the uneven

distributions of energy sources and demands, the impacts of severe weather on the resilience of MESs can differ at various nodes [20]. Therefore, new evaluation metrics need to be proposed to quantify the nodal resilience performance in different energy subsystems of MESs.

For calculating the resilience indices, the primary issue is to assess the energy losses of MESs at different time steps following the extreme event. The optimal power flow model aims to minimize the load curtailment costs to evaluate the electric losses during hurricanes. Ref. [22] proposes an optimal gas and power flow model to calculate the energy losses based on the minimization of gas and electric curtailment costs. For the optimal energy flow models in the previous studies, the total curtailment costs of energy carriers usually serve as the objection function without subdividing the specific services of different energy. Actually, the energy consumers in MESs are more focused on the energy-related service instead of different energy carriers. For example, the consumers are more concerned with the availability of space heating rather than where the heat comes from, e.g. produced through electrical heat pumps or directly from district heating networks. Under this circumstance, the energy-based optimal analysis model cannot characterize the identical service for different energy carriers, which may lead to impractical simulation results. Therefore, a service-based optimal energy flow model is necessary for practically evaluating the energy losses of MESs under windstorms.

In order to address the research gaps as aforementioned, this paper aims to evaluate the nodal resilience of MESs considering the interactions between different energy carriers, where the impacts of high winds on component and system operation are modeled during windstorms. The whole process of windstorms is divided into four phases: (i) pre-disturbance phase, (ii) disturbance progress phase, (iii) post-event degradation phase and (iv) system restoration phase. The innovative contributions of the study are summarized as:

- (1) A comprehensive framework is proposed to evaluate the impacts of windstorms on the resilience of MESs considering the interactions among different energy carriers. To model the time-dependent performance levels of MESs at different phases, the multi-phase performance response curve is utilized. Besides, the Monte-Carlo simulation (MCS) method is introduced to model the chaotic failures and restoration of components according to the weather extent.
- (2) Nodal resilience metrics for different energy subsystems are defined

to quantitatively evaluate the resilience of MESs. The proposed metrics include the expected energy losses, collapse ratio and recovery ratio, which can describe the expected level and instantaneous characteristics of resilience in MESs.

- (3) A modified optimal energy flow model is proposed to practically assess the energy losses of MESs considering the energy-related services of different consumers. The proposed model aims to minimize the total costs of energy services rather than energy carriers under windstorms by coordinating the energy production adjustment among different energy subsystems.

The remainder of the paper is organized as follows: Section 2 introduces the time-dependent resilience evaluation in MESs. The resilience of MESs under the impacts of windstorms at different phases is modeled in Section 3. The MCS-based simulation framework and resilience metrics of MESs are proposed in Section 4. Finally, case studies are described in Section 5, and the conclusion is given in Section 6.

## 2. Resilience evaluation of multi-energy systems under windstorms

### 2.1. The structure for multi-energy systems

The proposed MESs consist of electric system, natural gas system and energy hub (EH) [23], as shown in Fig. 1. The MESs have inputs of various energy (such as electricity and natural gas) from the common utilities and distribute them to energy consumers through electricity network and natural gas network [24]. Besides, the distributed energy resources (DERs) including solar photo-voltaic, wind and energy storage could provide immediate power for electric system. In the gas system, gas compressors are built to modify the suction or discharge pressures to maintain the pressure levels of pipelines. Regarding the interactions and couplings between different energy vectors, the EH is introduced where multiple energy carriers (i.e. electricity, gas and heat) can be converted [25]. The EH of MESs is composed of the combined heat and power (CHP) unit, power transformer, gas boiler and heat pump. The gas boiler is a device that generates heat through the consumption of natural gas. Due to different types of prime movers, the fuels applied for CHP units can differ, including natural gas, coals and etc. In this paper, one typical type of CHP unit with the gas turbine as prime movers is applied. The heat pumps are devices that usually

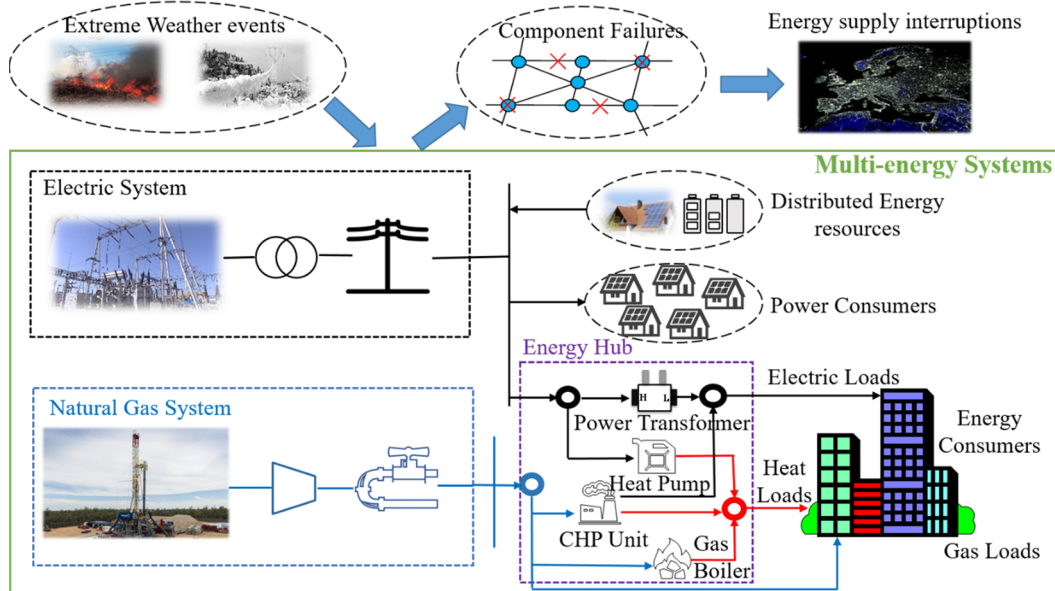


Fig. 1. Multi-energy systems architecture.

consume electricity to extract heat from a cold space and release it to a warmer one. The power transformer is built to step up and step down voltages when the electricity is transported from generation to demand. Therefore, the EH depicted in Fig. 1 is supplied by electricity and gas, while the electricity and heat are provided at the output port. Considering the cost, availability and related emissions of different energy carriers, the system operator could optimally dispatch the energy inputs to different elements of EH to provide efficient energy service for consumers.

Due to the impacts of extreme weather events such as windstorms, the occurrence of component failures can increase significantly, threatening the reliable operation of MESs [26]. Considering that gas pipelines are usually buried underground, only the impacts of high winds on the electric system are modeled in this paper. In the face of windstorms, the components in the electric system can suffer different kinds of damage. On the one hand, the overhead lines can be brought down due to bend down trees or fragile power poles caused by high winds. On the other hand, the heavy rain along with windstorms can cause the rise of water level, which may lead to the submergence of substations. Although the component failures caused by high winds can be local (i.e. only occur in the electric system), the operation of all the energy subsystems in MESs can be affected due to the interactions between different energy carriers. Under these circumstances, different energy including electricity, gas and heat supplied to consumers will be interrupted.

## 2.2. Illustration of resilience evaluation in multi-energy systems

In order to illustrate the resilience of the MESs, i.e. the ability of MESs to resist, absorb and recover from disruptive events, the multi-phase performance response curve is utilized to quantify the resilience level of MESs [12,16], as shown in Fig. 2. The performance response curve denotes the performance level change of MESs with time following the disturbance events. The performance levels of MESs  $\text{Per}(t)$  can be measured by different metrics, such as the number of functional components or the amount of energy supplied in the disasters.

Four phases can be seen in the multi-phase performance response curve of MESs of Fig. 2, namely [8]:

- (1) *Phase I*, pre-disturbance phase ( $t \in [0, t_0]$ ) represents that the disaster prevention of MESs from normal operation to the onset of random failures. In this phase, the initial performance level of MESs  $\text{Per}(t)$  is 100% before the disturbance events occur at  $t_0$ .
- (2) *Phase II*: disturbance progress phase ( $t \in [t_0, t_1]$ ) reflects the absorptive capacity of MESs to resist the impacts of initial failures. During this phase, the system operator will re-dispatch all the available resources (e.g. generation units, gas sources and energy loads) for the reliable operation of MESs. Under this circumstance, the performance level of MESs  $\text{Per}(t)$  can decrease from 100% to  $I$  when time  $t$  changes from  $t_0$  to  $t_1$ .
- (3) *Phase III*: post-event degraded phase ( $t \in [t_1, t_2]$ ) represents the time duration for designing the disaster recovery plan. In this phase, the performance level  $\text{Per}(t)$  resides at the post-disturbance degraded state  $I$  for some time before the restoration is initiated at  $t_2$ .
- (4) *Phase IV*: restoration phase ( $t \in [t_2, t_E]$ ) represents the recovery process of MESs during which the repair crews are dispatched to implement disaster recovery plans. With the restoration of damaged components, the performance level  $\text{Per}(t)$  of MESs will recover from  $I$  to the normal operation level 100%.

Based on the illustration of multi-phase performance response curve, the expected performance loss ( $EPL$ ) is defined to represent the resilience of MESs with the trapezoid area marked in a shadow of Fig. 2 [17], which can be expressed as:

$$EPL = \frac{\int_{t=0}^{t_E} [1 - \text{Per}(t)] dt}{\int_{t=0}^{t_E} dt} \quad (1)$$

The resilience indicator  $EPL$  describes the average performance losses of MESs considering both the intensity and duration of windstorms. Larger  $EPL$  values indicate lower resilience whereas smaller  $EPL$  values imply higher resilience [9]. Moreover, in order to describe the instantaneous variation of performance level in MESs, the collapse ratio  $CR$  in phase II and recovery ratio  $RR$  in phase IV are defined in this paper.

The collapse ratio  $CR$  in disturbance progress phase reflects how fast the performance levels of MESs drop, which can be calculated as:

$$CR = \frac{d[\text{Per}(t)]}{dt} \quad t \in [t_0, t_1] \quad (2)$$

The recovery ratio  $RR$  in restorative phase reflects how promptly the MESs can restore to its initial performance level, which can be calculated as:

$$RR = \frac{d[\text{Per}(t)]}{dt} \quad t \in [t_2, t_E] \quad (3)$$

## 2.3. The outline to evaluate the resilience of multi-energy systems

Based on the multi-phase performance response curve in Fig. 2, the outline to evaluate the resilience of MMESs is illustrated in Fig. 3. During all the phases of an event, the impacts of weather extent (i.e. wind speeds) on the component failures and the re-dispatch of MESs are modeled. In the pre-disturbance phase (i.e. phase I), the failure models of components are introduced to characterize their failure probability related to wind speeds. Due to the component failures caused by windstorms, a service-based optimal energy flow model is developed in the disturbance progress phase (i.e. phase II) to assess the performance losses of MESs. The duration of post-event degraded phase (i.e. phase III) is determined according to the intensity of component damage caused by windstorms. In the restoration phase (i.e. phase IV), the weather-related restoration model is applied to determine the repair time of components based on the damage intensity.

In order to model the chaotic failures influenced by severe weather, the MCS method is then introduced in this paper. For different initial disturbances sampled by the MCS method, the time-dependent performance levels of MESs at different phases can be determined using the previous resilience analysis model. On the basis, nodal resilience metrics for different energy subsystems can be calculated to quantify the regional resilience of MESs considering the impacts of windstorms, including the expected energy losses, collapse ratio and recovery ratio.

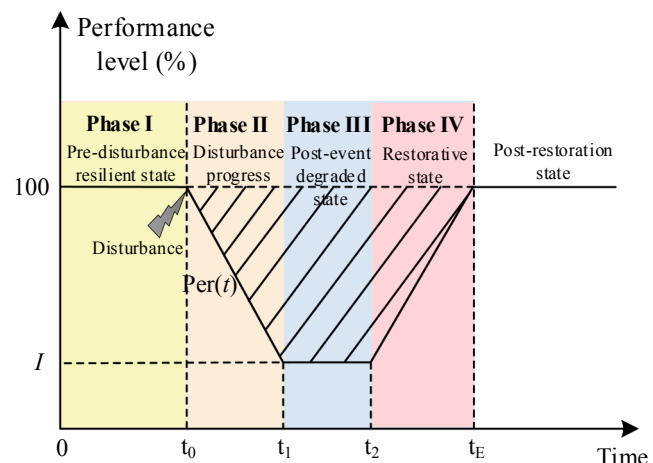


Fig. 2. Illustration of the multi-phase performance response curve of MESs.

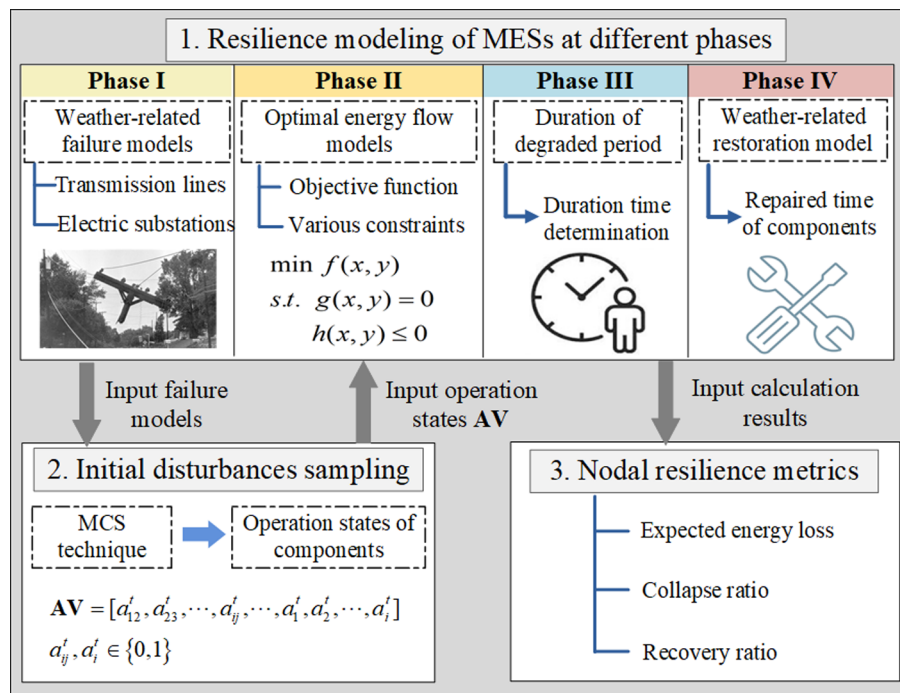


Fig. 3. The schematic diagram for illustrating the resilience evaluation of MESs.

The proposed metrics can describe the expected level and instantaneous characteristics of resilience in MESs. On the one hand, the expected energy losses are used as quantitative indicators to evaluate the average resilience performance of MESs under windstorms. On the other hand, the collapse and recovery ratios can capture the degradation and restoration features of resilience in MESs, i.e. how fast the system performance drops when the weather event hits MESs and how long the system recovers to its initial state, respectively.

### 3. Resilience modeling of MESs under windstorms

Due to the interactions between different energy carriers, the component failures caused by high winds in electric system can also lead to gas or heat interruptions in the other energy subsystems. Based on the previous illustration of multi-phase performance response curve of Fig. 2, the resilience of MESs is studied in this section.

#### 3.1. Phase I: pre-disturbance phase

During phase I, the MESs continue the normal operation until the disturbance events (i.e. windstorms) occur at  $t_0$ . Under the windstorms, the components in electric network can suffer different extents of damage due to their different working characteristics. Generally, the components in electric network can be classified as transmission lines (i.e. overhead lines, underground cables) and electrical substations. In this section, the failure models of different components considering the impacts of windstorms are illustrated.

##### (1) Failure model of overhead lines

In order to model the fragility of overhead lines to high winds, the fragility curve is introduced here, which characterizes the relationship between the failure probability of overhead lines and their surrounding weather extent (e.g. wind speeds) [16]. On the basis, the weather-dependent and time-dependent failure probability of overhead lines can be determined by mapping the profile of wind speed to the fragility curve. As illustrated in [4], a generic fragility curve is shown in Fig. 4, which can be expressed as:

$$p_{ij}^{over}(v) = \begin{cases} p_{ij}^0, & \text{if } v \leq v_{cri} \\ p_{ij\_v}(v), & \text{if } v_{cri} < v \leq v_{col} \\ 1, & \text{if } v > v_{col} \end{cases} \quad (4)$$

where  $p_{ij}^{over}(v)$  denotes the failure probability of overhead lines as the function of wind speed  $v$ ;  $p_{ij}^0$  denotes the failure probability of lines under good weather conditions;  $p_{ij\_v}(v)$  denotes the relation between failure probability and wind speed  $v$  from  $v_{cri}$  to  $v_{col}$ .

##### (2) Failure model of underground cables

In contrast to overload lines, the electric cables are usually buried underground, which are more resilient to windstorms. Therefore, the failure probability of underground cables has no relation with wind speeds, which can be calculated as:

$$p_{ij}^{cab}(v) = p_{ij}^{cab, 0} \quad (5)$$

where  $p_{ij}^{cab, 0}$  denotes the failure probability of cable  $ij$  under normal condition.

##### (3) Failure model of electrical substations

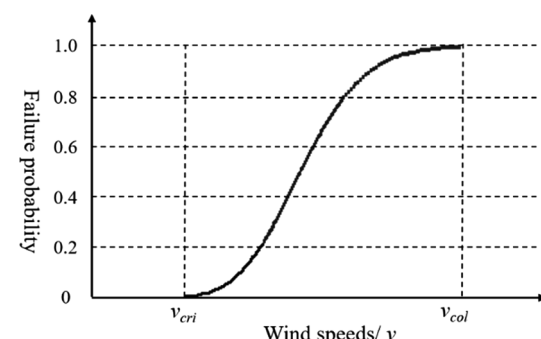


Fig. 4. A generic fragility curve showing the relation between failure probability of overhead lines and wind speed.

To characterize the vulnerability of electrical substations to high winds, the fragility functions are introduced in this paper, which model the relationship between the failure probability of substations and the weather extent. According to [27], the failure probability of substation  $i$  under the given wind speed can be evaluated using the following function:

$$p_i^{\text{subs}}(v) = \phi\left(\frac{\ln(v) - \mu}{\sigma}\right) \quad (6)$$

where  $\mu$  and  $\sigma$  are the logarithmic mean and the standard deviation, respectively. The set of parameters  $\mu$  and  $\sigma$  is related to the structural characteristics and layout of a substation. The estimation results of  $\mu$  and  $\sigma$  for different layouts of substations (open, suburban, light urban and etc.) are provided in [27]. Taking the suburban substation as an example, the values of  $\mu$  and  $\sigma$  in the fragility functions are 5.419 and 0.419, respectively. On the basis, the failure probability of a suburban substation for wind speed  $v$  can be determined using the fragility functions in (6).

#### (4) The availability of electrical components

To model the operation states of electrical components (i.e. lines and substations) considering the impacts of high winds at different time, the availability vector  $\mathbf{AV}$  is introduced here, which can be expressed as:

$$\mathbf{AV} = [a_{12}^t, a_{23}^t, \dots, a_{ij}^t, \dots, a_1^t, a_2^t, \dots, a_i^t] \quad a_{ij}^t, a_i^t \in \{0, 1\} \quad (7)$$

where  $a_{ij}^t$  denotes the operation state of overhead line  $ij$  or cable  $ij$  at time  $t$ ;  $a_i^t$  denotes the operation state of substation  $i$  at time  $t$ .

The operation states of electrical components can be either 0 or 1, where 1 corresponds to component connection and 0 corresponds to component outage. Besides, it should be noted that the operation states of components at time  $t$  are dependent on the operation states at the previous time steps. In specific, the component tripped at time  $t$  will stay failed in the following time steps since no repair crews are dispatched during windstorms for safety reasons [16]. Taking overhead line  $ij$  as an example, its operation state  $a_{ij}^t$  at time  $t$  can be determined based on the current failure probability and the previous operation states utilizing state sampling techniques [28].

$$a_{ij}^t = \begin{cases} a_{ij}^{t-1}.1, & \text{if } p_{ij}^{\text{over}}(v) \leq r \\ a_{ij}^{t-1}.0, & \text{if } p_{ij}^{\text{over}}(v) > r \end{cases} \quad (8)$$

where  $r$  is the random number sampled from the uniform distribution in the interval  $(0,1)$ , which can be represented as  $r \sim U(0, 1)$ . The variable  $r$  is generated to determine the operation state of line  $ij$ , which is not dependent on wind speed  $v$ . The impacts of weather conditions on the operation state of line  $ij$  can be embodied in the failure probability  $p_{ij}^{\text{over}}(v)$ .

#### 3.2. Phase II: disturbance progress phase

Due to the chaotic component failures caused by windstorms from  $t_0$  to  $t_1$ , the MESs will deviate from its normal operation state. Under this circumstance, re-dispatch of power generation and gas sources or load shedding will be adopted by system operators for the reliable operation

of MESs [20]. In order to minimize the consequences caused by windstorms, the modified optimal energy flow techniques in (9)–(29) are proposed in this paper to determine the re-dispatch results of MESs at different time  $t$ . In this paper, the performance levels of MESs  $\text{Per}(t)$  are measured by the percentage of electric loads, gas loads and heat loads connected to systems.

Considering the difference of energy services among consumers in different sectors, we categorize the consumers into residential, commercial, and industrial ones. Table 1 shows the primary services of different energy for different energy customer sectors based on the statistical data in [29,30]. Taking electricity as an example, the primary services of electricity for residential consumers are electronic appliances (e.g. TV) and lighting. Regarding commercial consumers, their electricity services mainly consist of heating and lighting. The industrial consumers mainly use electricity for product processing and heating.

Generally, the priority of energy demands can be converted into the corresponding interruption cost to shed loads. For example, the interruption costs of lighting can be larger than TV since the lighting is more important. Therefore, the objective function is to minimize the total costs of energy load curtailments at time  $t$ .

$$\begin{aligned} \text{Min} \quad & \left\{ \sum_{i=1}^N \sum_{s=1}^S \sum_{z=1}^Z [C_{isz}^t (\Delta P_{isz}^t) + C_{isz}^t (\Delta L_{isz}^t)] \right. \\ & \left. + \sum_{m=1}^M \sum_{s=1}^S \sum_{z=1}^Z [C_{msz}^t (\psi \cdot \Delta W_{msz}^t)] + \sum_{m=1}^M \sum_{s=1}^S C_{is}^t (\Delta h_{is}^t) \right\} \\ \text{where} \quad & P_{IL}^t = \sum_{s=1}^S \sum_{z=1}^Z \Delta P_{isz}^t, L_{ie}^t = \sum_{s=1}^S \sum_{z=1}^Z \Delta L_{isz}^t \\ & \Delta W_{mL}^t = \sum_{s=1}^S \sum_{z=1}^Z \Delta W_{msz}^t, \Delta L_{ih}^t = \sum_{s=1}^S \sum_{z=1}^Z \Delta h_{is}^t \end{aligned} \quad (9)$$

where  $\Delta P_{isz}^t$  and  $C_{isz}^t$  denote the electric load curtailment and the corresponding compensation cost (\$/MW) of consumer  $z$  in sector  $s$  at electric node  $i$  and time  $t$ , respectively.  $\Delta L_{isz}^t$  denotes the electric load curtailment of consumer  $z$  in sector  $s$  for the EH connected to electric node  $i$ .  $\Delta W_{msz}^t$  and  $C_{msz}^t$  denotes the gas load curtailment and the corresponding compensation cost (\$/m<sup>3</sup>) of consumer  $z$  in sector  $s$  at gas node  $m$  and time  $t$ , respectively.  $\Delta h_{is}^t$  and  $C_{is}^t$  denotes the heat load curtailment and the corresponding compensation cost (\$/MW) of consumers in sector  $s$  for the EH connected to electric node  $i$ .  $\psi$  denotes the gas gross heating value (MW/m<sup>3</sup>).  $\Delta P_{IL}^t$  denotes the total electric load curtailment at electric node  $i$  and time  $t$ .  $\Delta W_{mL}^t$  denotes the total gas load curtailment at electric node  $i$  and time  $t$ .  $\Delta L_{ie}^t$  and  $\Delta L_{ih}^t$  denote the electric and gas load curtailments of the EH connected to electric node  $i$  at time  $t$ , respectively.

The optimal energy flow also needs to satisfy the following constraints:

#### (a) Constraints of coupled components

The coupled relationship between different energy carriers in MESs can be described by coupled components. Generally, the coupled components in MESs can be classified into EH and electric-driven gas sources (EGSs). In this section, the operation models of coupled components are illustrated.

#### (a) Energy hub

The coupling relationship between inputs and outputs of EH is

**Table 1**

Illustration of the primary services of different energy for different energy customer sectors.

Consumer sector	Electricity	Gas	Heat
Residential	Lighting, electronic appliances	Heating, cooking	Heating
Commercial	Heating, lighting	Heating, equipment driving	Heating
Industrial	Product processing, heating	Product processing, heating	Heating

illustrated in Fig. 5, which can be expressed as [25]:

$$\begin{bmatrix} L_{ie}^0 - \Delta L_{ie}^t \\ L_{ih}^0 - \Delta L_{ih}^t \end{bmatrix} = \begin{bmatrix} \alpha_i^t & v_i^t \cdot \eta_e \cdot \psi \\ (1 - \alpha_i^t) \cdot \varphi & v_i^t \cdot \eta_h \cdot \psi + (1 - v_i^t) \cdot \theta_g \end{bmatrix} \cdot \begin{bmatrix} P_{i,EH}^t \\ F_{m,EH}^t \end{bmatrix} \quad (10)$$

where  $\alpha_i^t$  represents the dispatch factor of electricity flow.  $v_i^t$  represents the dispatch factor of gas flow.  $\eta_e$  and  $\eta_h$  represent the electrical efficiency and thermal efficiency of CHP, respectively.  $\varphi$  and  $\theta_g$  represent the efficiency of heat pump and gas boiler, respectively.  $L_{ie}^0$  and  $L_{ih}^0$  represent the electricity demand and heat demand of EH connected to electric node  $i$  in normal conditions, respectively.  $P_{i,EH}^t$  and  $F_{m,EH}^t$  represent the input electricity flow and gas flow to EH at time  $t$ , respectively.

The dispatch factor of EH is bounded by:

$$0 \leq \alpha_i^t \leq 1, \quad 0 \leq v_i^t \leq 1 \quad (11)$$

The energy load curtailments of EH are bounded by:

$$0 \leq \Delta L_{ie}^t \leq L_{ie}^0 \quad (12)$$

$$0 \leq \Delta L_{ih}^t \leq L_{ih}^0 \quad (13)$$

#### (b) Electric-driven gas sources

The EGSs in natural gas network need to get electric power supply from power system to maintain proper operation. Generally, the power consumption  $D_{ik}^t$  of EGS  $k$  is related to its gas production  $W_{mk}^t$ , which can be described as [20]:

$$D_{ik}^t = \eta_g \cdot W_{mk}^t \quad (14)$$

where  $\eta_g$  represents the conversion factor of EGSs (MW/m<sup>3</sup>).

Considering the impacts of windstorms, the power supply of EGS  $k$  at time  $t$  can be determined by the electric load curtailments at the corresponding nodes. In order to guarantee the reliable operation of EGSs, the power supplied to EGSs needs to be satisfied firstly during contingencies [13]. Therefore, the operation state  $\psi_{mk}^t$  of EGS  $k$  at gas node  $m$  and time  $t$  can be determined as:

$$\psi_{mk}^t = \begin{cases} 0, & \text{if } D_{ik}^t > D_{il}^0 - \Delta P_{il}^t \\ 1, & \text{if } D_{ik}^t \leq D_{il}^0 - \Delta P_{il}^t \end{cases} \quad (15)$$

where  $D_{il}^0$  denotes the initial electric load at electric node  $i$  in normal condition. It can be noted that EGS  $k$  will be interrupted when the power  $D_{il}^0 - \Delta P_{il}^t$  supplied to EGS is smaller than its power requirement  $D_{ik}^t$  for proper operation.

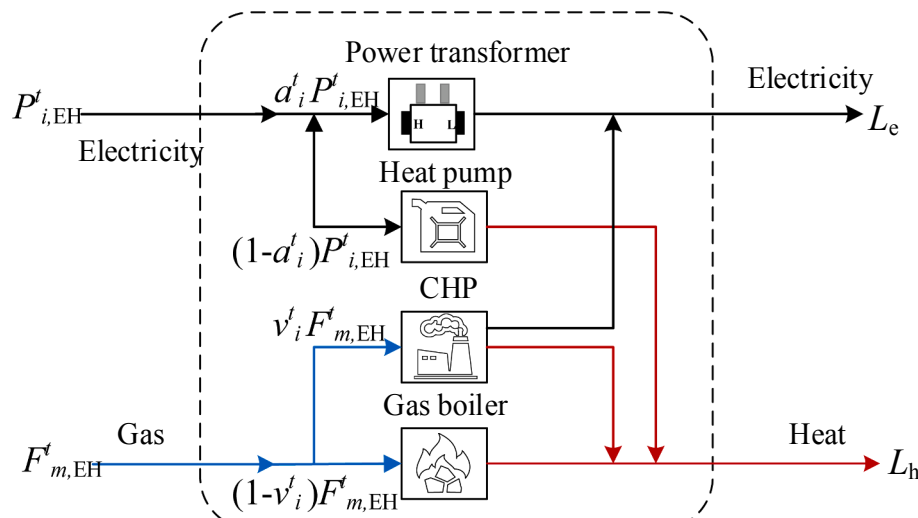


Fig. 5. The coupling relationship between inputs and outputs of the energy hub.

#### (1) Natural gas network constraints

A typical natural gas system consists of gas sources, pipelines and compressors from gas production to consumption [31]. In addition to EGSs, there are fuel-driven gas sources (FGSs) that can supply gas to consumers in natural gas system. During operation, these components need to satisfy the following constraints:

##### (a) Pipeline flow constraints

The gas flow  $f_{mn}^t$  through pipeline  $mn$  at time  $t$  can be calculated using the Weymouth equation [31], which can be expressed as:

$$|f_{mn}^t| \cdot f_{mn}^t = M_{mn} \cdot [(\pi_m^t)^2 - (\pi_n^t)^2] \quad (16)$$

where  $\pi_m^t$  and  $\pi_n^t$  represent the gas pressures of node  $m$  and node  $n$  at time  $t$ , respectively.  $M_{mn}$  denotes constant pipeline flow coefficient, which is related to the diameter and length of pipeline, pressure and temperature of gas.

The gas flow through pipeline  $mn$  is also restricted by its pipeline capacity:

$$f_{mn}^t \leq f_{mn}^t \leq f_{mn}^{\bar{t}} \quad (17)$$

where  $f_{mn}^{\bar{t}}$  and  $f_{mn}^t$  represent the maximum and minimum gas flow of pipeline  $mn$  at time  $t$ , respectively.

##### (b) Gas flow balance at each node

Similar to power system, the natural gas system needs to satisfy the constraint that the gas injected into a node must also flow out of the node, which can be expressed as:

$$\psi_{mk}^t \cdot W_{mk}^t + W_{ms}^t - (D_{ml}^0 - \Delta W_{ml}^t) - F_{m,EH}^t - \sum_{n=1}^M f_{mn}^t - \sum_{c=1}^{CO} f_c^t = 0 \quad (18)$$

where  $W_{mk}^t$  denotes the gas production of EGS  $k$  at node  $m$  and time  $t$ ;  $W_{ms}^t$  denotes the gas production of FGS  $s$  at node  $m$  and time  $t$ ;  $f_c^t$  denotes the gas flow through compressor  $c$  at time  $t$ ;  $CO$  refers to the total number of compressors.

##### (c) Compressor model

For compressor stations, the pressure  $\pi_m^t$  at the incoming node  $m$  can be proportional to the pressure  $\pi_n^t$  at out-coming node  $n$ , which is expressed as:

$$\pi_n^t = \tau_c^t \cdot \pi_m^t \quad (19)$$

$$\underline{\tau}_c^t \leq \tau_c^t \leq \bar{\tau}_c^t \quad (20)$$

where  $\tau_c^t$  denotes the compression ratio of compressor  $c$  at time  $t$ ;  $\bar{\tau}_c^t$  and  $\underline{\tau}_c^t$  represent the maximum and minimum compression ratios of compressor  $c$ , respectively.

#### (d) Gas pressure constraints

The pressure levels at each node are bounded by:

$$\underline{\pi}_m^t \leq \pi_m^t \leq \bar{\pi}_m^t \quad (21)$$

where  $\bar{\pi}_m^t$  and  $\underline{\pi}_m^t$  represent the maximum and minimum gas pressures at node  $m$  and time  $t$ , respectively.

#### (e) Gas source production constraints

The gas production of EGSs and FGSs is constrained by minimum and maximum levels, which can be expressed as:

$$\underline{W}_{ms}^t \leq W_{ms}^t \leq \bar{W}_{ms}^t \quad (22)$$

$$\underline{W}_{mk}^t \leq W_{mk}^t \leq \bar{W}_{mk}^t \quad (23)$$

where  $\bar{W}_{ms}^t$  and  $\underline{W}_{ms}^t$  represent the maximum and minimum production of FGS  $s$  at node  $m$  and time  $t$ , respectively;  $\bar{W}_{mk}^t$  and  $\underline{W}_{mk}^t$  represent the maximum and minimum production of EGS  $k$  at node  $m$  and time  $t$ , respectively.

#### (f) Gas load curtailment constraints

The gas load curtailment at each node is bounded by:

$$0 \leq \Delta W_{mL}^t \leq D_{mL}^0 \quad (24)$$

#### (2) Electric network constraints

Due to the impacts of component damages caused by windstorms, the power flow through electric system will be re-dispatched. Therefore, similar to natural gas system, the operation of electric system needs to satisfy the following constraints [32]:

##### (a) Power flow balance at each node

$$P_{ig}^t - (D_{IL}^0 - \Delta P_{IL}^t) - P_{i,EH}^t = \sum_{j=1}^N \frac{\theta_i^t - \theta_j^t}{x_{ij}^t} \quad (25)$$

##### (b) Generating unit limits

$$\underline{P}_{ig}^t \leq P_{ig}^t \leq \bar{P}_{ig}^t \quad (26)$$

##### (c) Line flow constraints

$$\left| \frac{\theta_i^t - \theta_j^t}{x_{ij}^t} \right| \leq a_{ij}^t \cdot \bar{S}_{ij}^t \quad (27)$$

##### (d) Bus phase constraints

$$\underline{\theta}_i^t \leq \theta_i^t \leq \bar{\theta}_i^t \quad (28)$$

##### (e) Electric load curtailment constraints

$$0 \leq \Delta P_{IL}^t \leq D_{IL}^0 \quad (29)$$

where  $P_{ig}^t$  represents the power output of generator  $g$  at node  $i$  and time  $t$ ;  $\theta_i^t$  represents the phase angle of node  $i$  at time  $t$ ;  $x_{ij}^t$  represents the reactance of line between node  $i$  and node  $j$ ;  $\bar{P}_{ig}^t$  and  $\underline{P}_{ig}^t$  represents the

maximum and minimum output of generators;  $\bar{S}_{ij}^t$  represents the power flow limits of line  $ij$ ;  $\bar{\theta}_i^t$  and  $\underline{\theta}_i^t$  represent the maximum and minimum of phase angle at node  $i$ .

The modified optimal energy flow model under windstorms can be formulated as the non-linear optimization problem in (9)–(29). However, due to the nonlinearity of pipeline equation in (16), the feasible region of the optimal energy flow model can be nonconvex which will challenge the global optimality. Therefore, the piecewise linearization techniques are introduced in this paper to linearize the pipeline equation [33]. Then, the proposed model is converted into a linear programming (LP) problem, which can be solved by the Cplex solver. The mathematical descriptions for the piecewise linearization of pipeline flow can be found in the Appendix A.

### 3.3. Phase III: post-event degraded phase

After the windstorm is ended at  $t_1$ , the system operator will start to make recovery measures about how the MESs are restored. Besides, the restoration resources need to be allocated, including repair crews, vehicles, equipment and some replacement components [12]. In this phase, the performance level of MESs resides at the post-disturbance degraded state  $I$  until the restoration is initiated at  $t_2$ . Generally, the duration of post-event degraded period is related to the extent of component damages caused by windstorms [16]. If the windstorms affect wider areas or lead to larger losses in MESs, the time needed for the implementation of recovery measures can be relatively longer.

In order to characterize the impacts of component damage on the measure-making, the duration of post-event degraded period  $t_2 - t_1$  can be assumed as the function of wind speed  $v$  [16], which is expressed as:

$$t_2 - t_1 = \phi(v) \cdot T_d^{normal} \quad (30)$$

where  $T_d^{normal}$  refers to the mean time needed for measure-making under normal weather, which is assumed to be 3 h.  $\phi(v)$  is multiplying operator to model the positive relationship between period duration and wind speeds.

### 3.4. Phase IV: Restoration phase

Based on the predetermined recovery measures in phase III, the restoration of MESs is initiated at  $t_2$ . It should be illustrated that no restoration is implemented during windstorms due to safety reasons, so the repair crews are dispatched only in the restoration phase [16]. Moreover, it will take more time for repair crews to restore the damaged components for higher wind speeds [14]. Therefore, a weather-related restoration model is introduced to calculate the repair time of damaged components  $TTR$ :

$$TTR = \varphi(v) \cdot MTTR^{normal} \quad (31)$$

where  $MTTR^{normal}$  denotes the mean time to repair damaged components under normal weather, which is assumed to be 2 h for lines and 8 h for substations.  $\varphi(v)$  represents the multiplying operator to model the increasing repair time for higher component damage caused by larger wind speeds.

During restorative phase from  $t_2$  to  $t_E$ , this paper adopts a random restoration strategy, where the damaged lines and substations are randomly selected to repair. For time  $t$  in the phase III, the damaged component for repair and its corresponding repair time  $TTR$  will be determined utilizing state sampling techniques. Therefore, the performance levels of MESs at time  $t$  can then be evaluated.

#### 4. Framework for resilience evaluation of MESs utilizing Monte Carlo simulation

##### 4.1. Nodal resilience metrics

According to the illustration of multi-phase performance response curve in [Section 2.2](#), different metrics are defined to quantify the nodal resilience of MESs under windstorms, including the expected energy load curtailments, the collapse ratio and the recovery ratio of energy supply level [\[16\]](#). After the simulation, the expected electric load curtailments ( $EELC_i$ ) at electric node  $i$ , expected gas load curtailments ( $EGLC_m$ ) at gas node  $m$  and expected heat load curtailments ( $EHLC_i$ ) at electric node  $i$  in MESs for  $t \in [0, t_E]$  can be calculated as:

$$EELC_i = \sum_{st=1}^{ST} \left[ \sum_{b=0}^{t_E/\Delta t} \left( \frac{\Delta P_{il}^{b\cdot\Delta t} + \Delta L_{ie}^{b\cdot\Delta t}}{D_{il}^0 + L_{ie}^0} \right) \cdot \Delta t / t_E \right] / ST \quad (32)$$

$$EGLC_m = \sum_{st=1}^{ST} \left[ \sum_{b=0}^{t_E/\Delta t} \frac{\Delta W_{ml}^{b\cdot\Delta t}}{D_{ml}^0} \cdot \Delta t / t_E \right] / ST \quad (33)$$

$$EHLC_i = \sum_{st=1}^{ST} \left[ \sum_{b=0}^{t_E/\Delta t} \frac{\Delta L_{ih}^{b\cdot\Delta t}}{L_{ih}^0} \cdot \Delta t / t_E \right] / ST \quad (34)$$

where  $\Delta t$  denotes the time interval for the resilience re-evaluation of MESs, which is assumed as 1 h.  $b$  denotes the total number of re-evaluation, which equals to  $t_E/\Delta t$ .  $ST$  represents the total simulation times of MCS.

After obtaining the expected energy load curtailments at different nodes, system  $EELC$ ,  $EGLC$  and  $EHLC$  can be calculated based on the following equations:

$$EELC = \sum_{st=1}^{ST} \left[ \sum_{b=0}^{t_E/\Delta t} \sum_{i=1}^N \left( \frac{\Delta P_{il}^{b\cdot\Delta t} + \Delta L_{ie}^{b\cdot\Delta t}}{D_{il}^0 + L_{ie}^0} \right) \cdot \Delta t / t_E \right] / ST \quad (35)$$

$$EGLC = \sum_{st=1}^{ST} \left[ \sum_{b=0}^{t_E/\Delta t} \sum_{m=1}^M \frac{\Delta W_{ml}^{b\cdot\Delta t}}{D_{ml}^0} \cdot \Delta t / t_E \right] / ST \quad (36)$$

$$EHLC = \sum_{st=1}^{ST} \left[ \sum_{b=0}^{t_E/\Delta t} \sum_{i=1}^N \frac{\Delta L_{ih}^{b\cdot\Delta t}}{L_{ih}^0} \cdot \Delta t / t_E \right] / ST \quad (37)$$

To quantify the overall resilience of MESs, the synthetic energy loss ( $SEL$ ) is proposed by incorporating the load curtailments in different energy subsystems. After unifying the units of electricity, gas and heat, the  $SEL$  of MESs can be calculated using the following equation:

$$SEL = \frac{EELC \cdot \sum_{i=1}^N (D_{il}^0 + L_{ie}^0) + \psi \cdot EGLC \cdot \sum_{m=1}^M D_{ml}^0 + EHLC \cdot \sum_{i=1}^N L_{ih}^0}{\sum_{i=1}^N (D_{il}^0 + L_{ie}^0) + \psi \cdot \sum_{m=1}^M D_{ml}^0 + \sum_{i=1}^N L_{ih}^0} \quad (38)$$

where  $\psi$  denotes gas gross heating value.

Regarding the instantaneous variation of system energy supply level, the collapse ratios and recovery ratios in MESs are defined. During disturbance progress for  $t \in [t_0, t_1]$ , the collapse ratio of electricity ( $CRE$ ), gas ( $CRG$ ) and heat ( $CRH$ ) supply level can be calculated using the difference methods [\[34\]](#), which can be expressed as:

$$CRE = \sum_{st=1}^{ST} \left[ \sum_{b=1}^{(t_1-t_0)/\Delta t} \frac{\sum_{i=1}^N (\Delta P_{il}^{t_0+(b-1)\cdot\Delta t} + \Delta L_{ie}^{t_0+(b-1)\cdot\Delta t} - \Delta P_{il}^{t_0+b\cdot\Delta t} - \Delta L_{ie}^{t_0+b\cdot\Delta t}) / \Delta t}{(t_1 - t_0) / \Delta t} \right] / ST \quad (39)$$

$$CRG = \sum_{st=1}^{ST} \left[ \sum_{b=1}^{(t_1-t_0)/\Delta t} \frac{\sum_{m=1}^M (\Delta W_{ml}^{t_0+(b-1)\cdot\Delta t} - \Delta W_{ml}^{t_0+b\cdot\Delta t}) / \Delta t}{(t_1 - t_0) / \Delta t} \right] / ST \quad (40)$$

$$CRH = \sum_{st=1}^{ST} \left[ \sum_{b=1}^{(t_1-t_0)/\Delta t} \frac{\sum_{i=1}^N (\Delta L_{ih}^{t_0+(b-1)\cdot\Delta t} - \Delta L_{ih}^{t_0+b\cdot\Delta t}) / \Delta t}{(t_1 - t_0) / \Delta t} \right] / ST \quad (41)$$

Similarly, the recovery ratio of electricity ( $RRE$ ), gas ( $RRG$ ) and heat ( $RRH$ ) supply level for  $t \in [t_2, t_E]$  can be calculated as:

$$RRE = \sum_{st=1}^{ST} \left[ \sum_{b=1}^{(t_E-t_2)/\Delta t} \frac{\sum_{i=1}^N (\Delta P_{il}^{t_2+b\cdot\Delta t} + \Delta L_{ie}^{t_2+b\cdot\Delta t} - \Delta P_{il}^{t_2+(b-1)\cdot\Delta t} - \Delta L_{ie}^{t_2+(b-1)\cdot\Delta t}) / \Delta t}{(t_E - t_2) / \Delta t} \right] / ST \quad (42)$$

$$RRG = \sum_{st=1}^{ST} \left[ \sum_{b=1}^{(t_E-t_2)/\Delta t} \frac{\sum_{m=1}^M (\Delta W_{ml}^{t_2+b\cdot\Delta t} - \Delta W_{ml}^{t_2+(b-1)\cdot\Delta t}) / \Delta t}{(t_E - t_2) / \Delta t} \right] / ST \quad (43)$$

$$RRH = \sum_{st=1}^{ST} \left[ \sum_{b=1}^{(t_E-t_2)/\Delta t} \frac{\sum_{i=1}^N (\Delta L_{ih}^{t_2+b\cdot\Delta t} - \Delta L_{ih}^{t_2+(b-1)\cdot\Delta t}) / \Delta t}{(t_E - t_2) / \Delta t} \right] / ST \quad (44)$$

##### 4.2. Simulation procedures

As illustrated in [Fig. 6](#), the procedures for resilience evaluation of MESs can be divided into four steps. The first step is the initialization of MESs, where the initial parameters are set. On the basis, the initial operation states of MESs can be obtained.

The second step is the resilience simulation of MESs considering the impacts of windstorms with  $\Delta t$  temporal resolution from 0 to  $t_E$ . As illustrated in [Section 2.2](#), the process for the resilience evaluation of MESs consists of four phases. During phase I for  $t \in [0, t_0]$ , the MESs continue normal operation until the windstorms occur at  $t_0$ . The failure probability of overhead lines, underground cables and electrical substations can be determined according to wind speeds using [\(4\)](#), [\(5\)](#) and [\(6\)](#), respectively. During phase II for  $t \in [t_0, t_1]$ , the operation states of electrical components  $AV$  can be obtained using MCS techniques. For certain component failures, the energy supply levels of MESs can be calculated using the optimal energy flow model in [\(9\)–\(29\)](#). During phase III for  $t \in [t_1, t_2]$ , the MESs will reside at the post-disturbance degraded state until the recovery measure is initiated at  $t_2$ . The time duration  $t_2 - t_1$  of phase III can be determined using [\(30\)](#) according to wind speeds. During phase IV for  $t \in [t_2, t_E]$ , the damaged component for repair and its corresponding repair time  $TTR$  can be determined using [\(31\)](#). Considering the implementation of recovery measures, the energy supply restoration of MESs can be calculated using the optimal energy flow model in [\(9\)–\(29\)](#). On the basis, the energy supply levels of MESs under windstorms can be characterized as the function of time  $t$ .

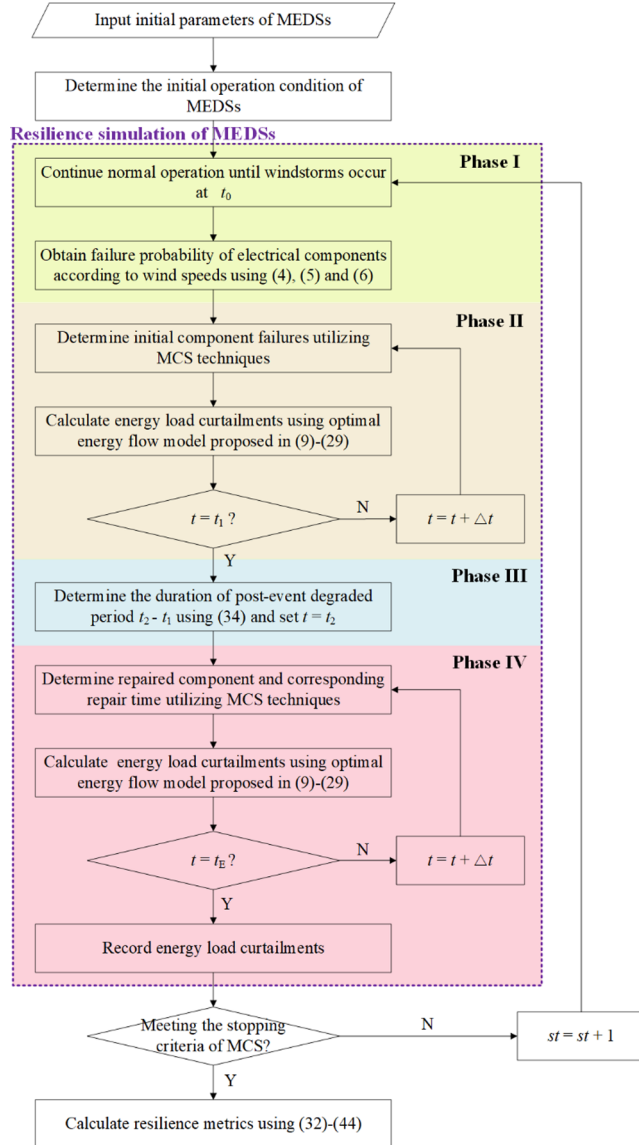


**Fig. 6.** Simulation procedures for resilience evaluation of MESs utilizing MCS technique.

The third step is to repeat the previous procedures until the stopping criterion of MCS technique is satisfied. The stopping criterion provided for MCS technique is the variation coefficient of resilience metrics, which can be calculated as:

$$\xi = \max(\sqrt{V(EELC)}/EELC, \sqrt{V(EGLC)}/EGLC, \sqrt{V(EHLC)}/EHLC) \quad (45)$$

where  $V(EELC)$ ,  $V(EGLC)$  and  $V(EHLC)$  are the variances of  $EELC$ ,  $EGLC$  and  $EHLC$ , respectively.

Based on the energy load curtailments for each simulation time, the fourth step is to calculate the resilience metrics of MESs using (32)–(44).

## 5. Case studies and discussions

### 5.1. Descriptions of test systems and simulation data

The proposed techniques and models are applied to evaluate the

resilience of MESs composed of IEEE 33-bus system from [1] and 20-node gas system detailed in [35], as shown in Fig. 7. The IEEE 33-bus electric system is composed of 7 generating nodes, 32 load nodes, 37 lines and 6 DERs. The lines 23–24, 24–25, 14–15, 16–17, 4–5 and 8–9 are assumed as underground cables. On the other hand, the 20-node gas system has two EGSSs, one FGS, three gas compressors and 19 pipelines. The EGSSs W1 and W2 at gas nodes 8 and 5 are supplied from power flow at electric nodes 18 and 19. In addition, there are 7 EHs which are plugged to electric nodes 24, 25, 7, 8, 30, 14, 33 in electric network and gas nodes 6, 7, 15, 16, 12, 19, 20 in gas network.

The physical parameters of gas compressors (such as maximum and minimum compression ratio), pipelines (such as diameter and length) and gas sources (such as production capacity) can be found in [35]. The generating capacity of DERs in electric network is set as 1 MW. Regarding EH, the electrical efficiency  $\eta_e$  and thermal efficiency  $\eta_h$  of CHP are 0.4 and 0.45, respectively [36]. The heat pump efficiency  $\varphi$  is assumed to be 3 [36]. The efficiency of gas boiler  $\eta_g$  is assumed as 0.85. The heat demand  $L_{ih}^0$  of EH at node  $i$  is assumed to be 0.9 time of the corresponding electricity demand  $L_{ie}^0$ . The gas gross heating value  $\psi$  is set as 8.4 KW/m<sup>3</sup> [20].

Based on the categories of energy services in Table 1, it is assumed that the proportions of residential, commercial and industrial consumers at each node are 35%, 35% and 30%, respectively. The proportions of electricity and gas services are set as 50% in the respective customer sectors. The interruption costs of the energy services for different customer sectors are shown in Table 2, which are assumed according to the analysis results in [20]. It should be noted that the compensation costs are identical for electricity, gas and heat with the same services. For instance, since the electricity and heat can both be used for heating in the commercial sectors, their compensation costs are identical. Besides, the units of gas interruption costs are converted into \$/10<sup>3</sup>m<sup>3</sup> using gas gross heating value  $\psi$ .

Regarding the resilience evaluation of MESs, the wind fragility curves of overhead lines can be found in [16]. The overhead line failure probability can be determined with the fragility curves for higher wind speeds ( $v > 20$  m/s) whereas the line normal failure probability 0.005 is used for normal weather conditions ( $v \leq 20$  m/s) [13]. The failure probability of underground cables is assumed to be 0.005. It is assumed that all the components are online at the beginning of simulation until the windstorms hit MESs at 10 h. The duration  $t_1 - t_0$  of windstorms is assumed to be 12 h, with an hourly time  $\Delta t$  resilience re-evaluation of MESs. During phase III, the mean time  $T_d^{normal}$  needed for measurement-making under normal weather is assumed as 3 h. During phase IV, the mean time to repair damaged lines and substations under normal weather  $MTTR^{normal}$  is assumed as 2 h and 8 h.

The hourly time scale  $\Delta t$  is selected to make a balance between simulation accuracy and computation time [4]. In specific, the time scales for assessing the resilience of MESs are closely related to the different characteristics of electricity and gas networks as well as the EH [37]. Generally, the time scale for assessing the resilience of the electric network can become much smaller than that for a CHP unit of EH. Nevertheless, the computation burden can also increase significantly with the decrease of time scales. Therefore, the time scales to evaluate the resilience of MESs are set as one hour by weighing up accuracy and efficiency. Moreover, it should be noted that a smaller time scale can be adopted in the proposed framework if required.

### 5.2. Case studies

In order to model the spatial characteristics of windstorms, the IEEE 33-bus system is arbitrarily divided into three weather region areas with different wind speeds  $v_1$ ,  $v_2$  and  $v_3$ , as shown in Fig. 7. As illustrated in Table 3, two cases with different types of windstorms are modeled in this paper considering the spatial characteristics of storms.

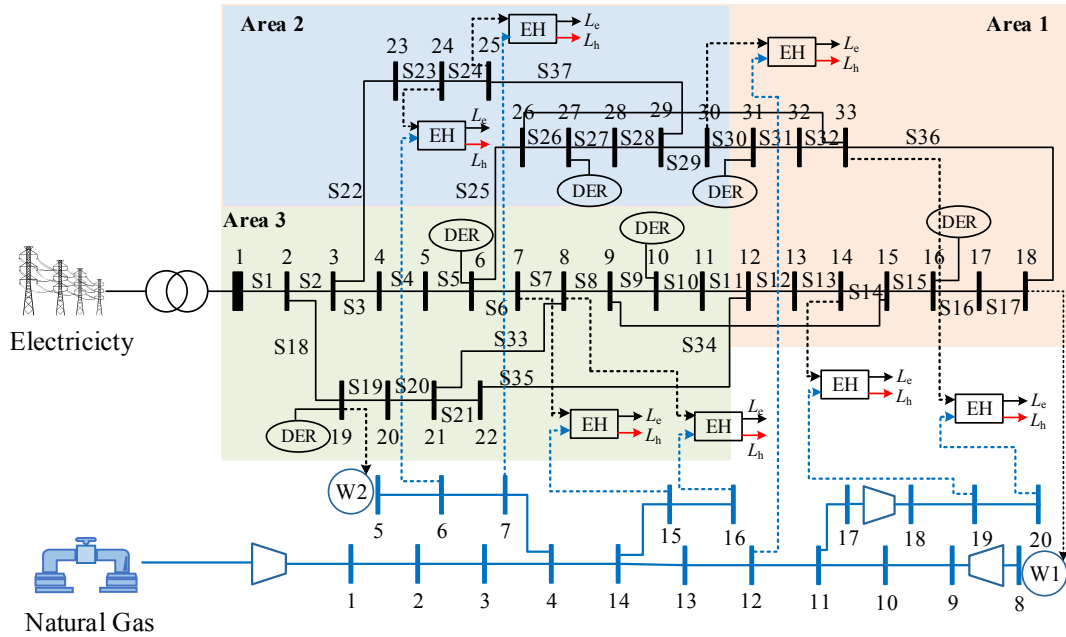


**Fig. 7.** Test system composed of IEEE 33-bus system and 20-node gas system.

In case 1, the resilience of MESs under the wide grid-scale windstorms is evaluated, where the wind speeds in the three areas of the test system are the same. Case 2 aims to quantitatively analyze the resilience of MESs considering the impacts of region-scale windstorms. Particularly, the wind speeds in the three areas of the test system are different. The formulation of resilience evaluation of MESs is accomplished by Matlab R2018b. The following cases are tested by a PC with Intel 3 GHz 4-core processor (6 MB L3 cache), 8 GB memory.

#### 5.2.1. Case 1: Resilience evaluation of MESs under the impacts of grid-scale windstorms

In this case, the wind speeds in three areas are the same and three scenarios with different weather extents  $v$  are analyzed, including 31 m/s, 36 m/s and 41 m/s wind speeds. The wind speeds in the three scenarios are selected according to the classification of storms, which can be found in [13]. In practical application, the wind speeds of storms can be preset by readers as required. According to the fragility curves in [13], the failure probability of overhead lines is 0.05, 0.10 and 0.20 corresponding to 31 m/s, 36 m/s and 41 m/s wind speeds, respectively.

In order to model the increasing repair time due to wind speeds, the multiplying operator  $\varphi(v)$  is determined by uniformly sampling within a pre-determined range (i.e.  $\varphi(v) \sim [h_1, h_2]$ ). In this application, the range  $[h_1, h_2]$  is  $[2, 3]$  for  $30 \leq v \leq 40$  and  $[3, 4]$  for higher wind speeds. Similarly, the multiplying operator  $\phi(v)$  in can be determined utilizing uniformly sampling techniques to model the impacts of wind speeds on the duration of phase III  $t_2 - t_1$ .

The electricity, gas and heat supply level considering the impacts of windstorms for different wind speeds (i.e. 31 m/s, 36 m/s and 41 m/s) are given in Fig. 8. It can be noted that the shapes of the energy supply

level curves recall the response curve of Fig. 2, where the four phases of resilience evaluation can be distinguished: pre-disturbance phase, disturbance progress, post-event degraded phase, and restoration phase. Based on the variation of energy supply levels with time in Fig. 8, the nodal resilience indices ( $EELC_i$ ,  $EGLC_m$  and  $EHLC_i$ ) for different wind speeds are presented in Fig. 9. It should be noted that only the resilience values associated with the energy nodes can be obtained via the simulation. With respect to the remaining points, their resilience values are estimated based on the obtained values at different energy nodes using interpolation methods. From subpictures (a)–(c) of Fig. 9, it can be noted that there are huge differences between nodal resilience indices at different nodes. Taking the electric system as an example, the values of  $EELC_i$  at electric node 21 are the largest among all nodes, which are 0.344, 0.599 and 0.796 for 31 m/s, 36 m/s and 41 m/s wind speeds, respectively. In contrast, the values of  $EELC_i$  at electric nodes 30, 8 and 9 are relatively small for all scenarios. This is mainly because that the demands at electric nodes 30, 8 and 9 can obtain electricity supply from EH under severe weather.

Besides, we also sort the nodal resilience indices  $EELC_i$  and  $EGLC_m$  from the biggest to the smallest, as shown in Fig. 10. The electric nodes with top 50% of  $EELC_i$  and the gas nodes with top 30% of  $EGLC_m$  are marked with node number. This is mainly because that these nodes with larger demands are relatively far away from energy resources. Under this circumstance, the power is more difficult to be transported from generators to consumers under windstorms, considering the operating constraints of power system. It can be noted that the increase of wind speeds has relatively small impacts on the ranking of nodal resilience indices in both gas and power systems. For example, the electric nodes with the top three nodal  $EELC_i$  in power system are all nodes 21, 22 and

**Table 2**

The interruption costs of energy services for different energy customer sectors.

Consumer sector	Electricity (\$/MW)	Gas(\$/10 <sup>3</sup> m <sup>3</sup> )	Heat(\$/MW)
Residential	Lighting (5000), electronic appliances (4000)	Heating (4000/8.4), cooking (5000/8.4)	Heating (4000)
Commercial	Heating (8000), lighting (10000)	Heating (8000/8.4), equipment driving (10000/8.4)	Heating (8000)
Industrial	Product processing (5000), heating (4000)	Product processing (5000/8.4), heating (4000/8.4)	Heating (8000)

**Table 3**  
Illustration of the two cases with different types of windstorms.

Cases	Types of windstorms	Characteristics of windstorms
Case 1	Grid-scale windstorm	The same wind speeds in three areas ( $v_1 = v_2 = v_3$ )
Case 2	Region-scale windstorm	Different wind speeds in three areas ( $v_1 \neq v_2 \neq v_3$ )

20. The findings can help us improve the resilience of MESs through hardening the electrical components at nodes with larger resilience indices.

The system resilience metrics of different energy carriers for different wind speeds are presented in Fig. 11. It can be clearly seen that the increase of wind speeds can significantly reduce the system resilience of MESs. For storms with larger wind speeds, the expected energy load curtailments and the collapse ratios both increase significantly, whereas the recovery ratios tend to decrease. The values of *EGLC* are 0.099, 0.234 and 0.368 for 31 m/s, 36 m/s and 41 m/s wind speeds, respectively, indicating that more gas loads will be interrupted for larger weather extent. When wind speeds  $v$  change from 31 m/s to 41 m/s, the values of *CRG* increase from 0.038 to 0.061, whereas the values of *RRG* decrease from 0.006 to 0.003. This means that the MESs will break down more rapidly in phase II and recover to normal operation more slowly in phase IV for higher wind speeds.

Regarding the comparison of system resilience between different energy carriers, we can find that the losses of heat supply caused by windstorms are smaller than those of power supply and gas supply, indicating the heat system is relatively more resilient to windstorms than the other two systems. As shown in Fig. 8, there is 88.1% of heat loads supplied by MESs after the attacks of storms with 41 m/s wind speed, whereas there are only 53.8% electricity loads and 39.2% gas loads connected after windstorms. Moreover, the values of *CRH* are much smaller than those of *CRE* and *CRG* for different wind speeds. This is mainly because that the heat demands of MESs are simultaneously supplied by electricity and gas through EH. When the power system cannot supply sufficient electricity to heat pump of EH for contingency states, the gas system can increase gas injection to CHP units and gas boiler of EH to satisfy heat demands.

In this case, the system resilience of MESs and isolated electric system (IES) under different wind events is also compared. As seen in the subpicture (a) of Fig. 8, the power system in MESs is more resilient than IES under the same windstorms, which is shown in the expected energy losses, collapse ratios and recovery ratios. The subpicture (a) of Fig. 11 illustrates the comparison of resilience metrics between MESs and IES for different wind speeds. Firstly, the windstorms can cause more electricity load losses in IES than those in MESs. For storms with 41 m/s wind speed, the *EELC* in IES can reach 0.696, which is over two times than that in MESs with value of 0.289. Moreover, the MESs can

better resist disruptive events in phase II and more quickly recover from degraded state in phase IV compared to IES. For instance, the values of *CRE* in IES are nearly two times than those in MESs for 31 m/s, 36 m/s and 41 m/s wind speeds. The main reason to account for this phenomenon is that the gas system can increase gas injection to CHP units of EH to satisfy the electric demands in MESs for contingency states.

To further show the impacts of energy interaction on the overall resilience of MESs, the synthetic energy loss (*SEL*) of MESs is compared with that of isolated energy subsystems (IES) for different wind speeds, as shown in Table 4. It can be noted that the energy interaction can improve the resilience of MESs for smaller wind speeds, since the *SEL* values of MESs and IESS are 0.0795 and 0.0934 for  $v = 31$  m/s, respectively. In contrast, the resilience of MESs can be reduced compared to IESS for larger wind speeds due to the interaction between different energy carriers. This is mainly because that the EGSSs can obtain sufficient power supply in most time of phase I when MESs are hit by storms with small wind speeds. Under this circumstance, the gas system can provide adequate gas for EH to produce electricity and heat for MESs. Instead, for storms with larger wind speeds, the EGSSs may stop working due to inadequate power supply at the beginning of phase I. Due to the reduction of gas supply, the EH will correspondingly reduce the energy production for MESs.

The computation time for the resilience evaluation of MESs for different wind speeds is shown in Table 5 to show the efficiency of the proposed method. It can be noted that the average computation time of the optimal energy flow model ranges from 4 s to 5 s for all wind speeds. Nevertheless, the total computation time for obtaining the results increases a lot with the increase of wind speeds. This is mainly because that the MESs can recover quickly to normal operation level in phase III for smaller wind speeds. Under this circumstance, the average number to calculate the optimal power flow per sample is relatively small for 31 m/s wind speeds.

#### 5.2.2. Case 2: Resilience analysis of MESs under the impacts of region-scale windstorms

In order to model the region-scale windstorms, the windstorms are assumed to only hit one area of the test system in Fig. 7. On the basis, the initialization of wind speeds in different areas is given in Table 6. Firstly, it should be noted that  $v = 20$  m/s corresponds to normal weather conditions with 0.005 line failure probability. Therefore, the

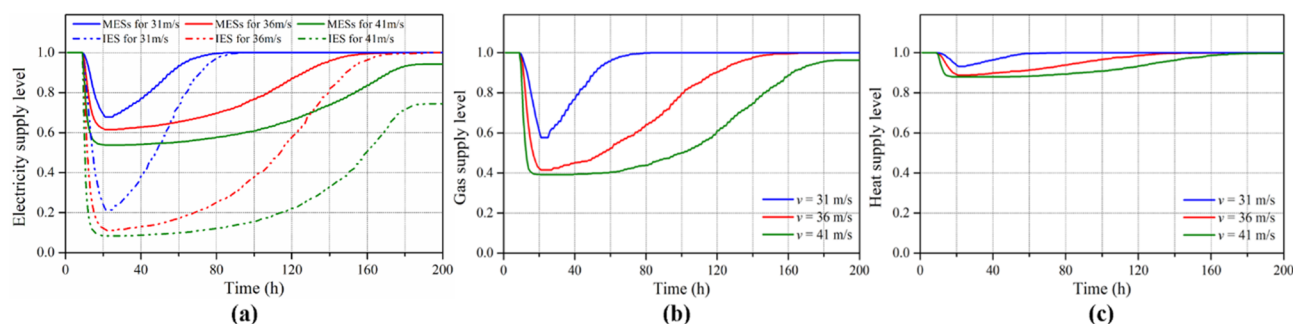


**Fig. 8.** Energy supply level of MESs as a function of time for different wind speeds. (a) Electricity supply level. (b) Gas supply level. (c) Heat supply level.

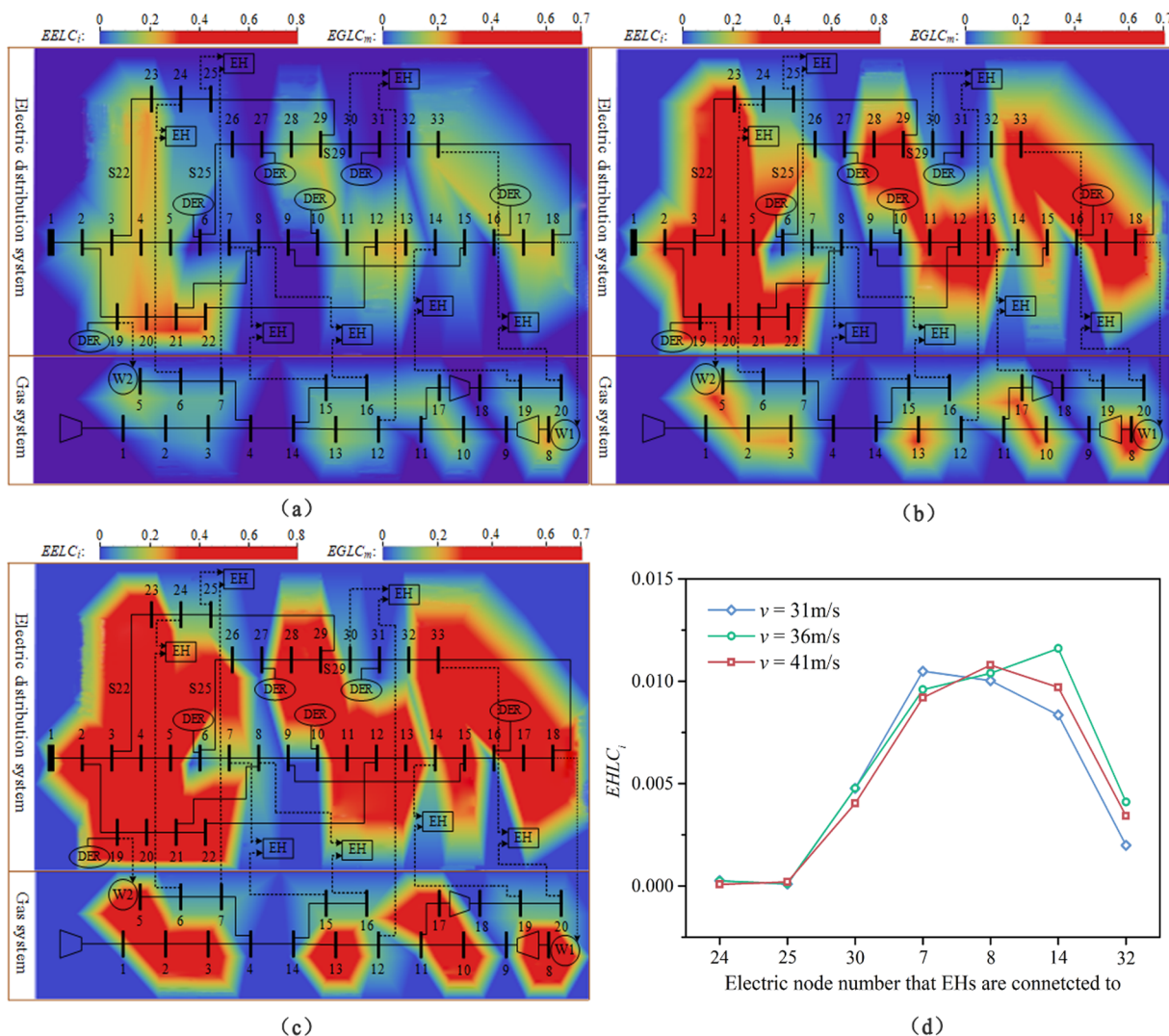


**Fig. 9.** Expected energy load curtailments at different nodes for different wind speeds. (a–c) Heat maps of MESs showing the distribution of nodal  $EELC_i$  and  $EGLC_m$  for 31 m/s, 36 m/s and 41 m/s wind speeds, respectively (d) Nodal  $EHLC_i$  for different wind speeds.

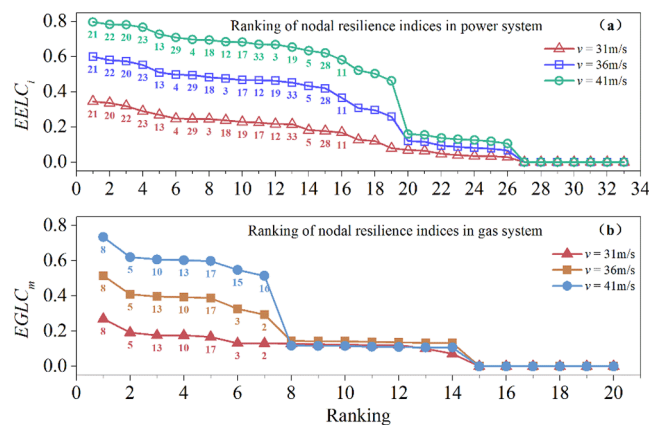


**Fig. 10.** Ranking of nodal resilience indices for different wind speeds. (a) Ranking of nodal  $EELC_i$  (b) Ranking of nodal  $EGLC_m$ .

windstorms are assumed to only hit areas 1, 2 and 3 of MESs corresponding to scenarios A, B and C, respectively. Moreover, there also exist region-scale windstorms whose wind speeds in different areas can differ. As shown in scenario D, the wind speeds of storms are therefore assumed as 41 m/s, 31 m/s and 20 m/s for areas 1, 2 and 3,

respectively. Besides, the techniques to determine the repair time TTR of damaged components and the duration of phase III are in accordance with those in case 1.

The electricity, gas and heat supply levels considering the impacts of windstorms for different scenarios are given in Fig. 12. Similar to case 1, the shapes of the energy supply level curves recall the response curve of Fig. 2. On the basis, the resilience metrics for different scenarios are given in Table 7. Regarding electric system, it can be noted that more electric losses are caused when windstorms hit area 3. The values of  $EELC$  in MESs are 0.0391, 0.0402, 0.1163 and 0.0819 for scenarios A, B, C and D, respectively. This is mainly because that the DERs in area 3 account for nearly 50% of total generation capacity. Regarding natural gas system, the simulation results of scenario A show that the windstorms can lead to more gas losses when windstorms hit area 1. The value of EGNS is only 0.0543 for scenario C and increases to 0.1731 for scenario A. This is mainly because that the electric-driven gas source W2 at node 8 accounts for over 50% production capacity in natural gas system. The windstorms in area 3 can lead to the interruption of power supplied to W2. In accordance with case 1, there is only a small fraction of heat losses caused by windstorms for all scenarios in case 2.

Based on the simulation results in Table 7, we can draw the conclusion that the resilience in the area 3 of MESs is the lowest considering the impacts of region-scale windstorms. Therefore, it is an effective measure to harden electrical components in area 3 for improving

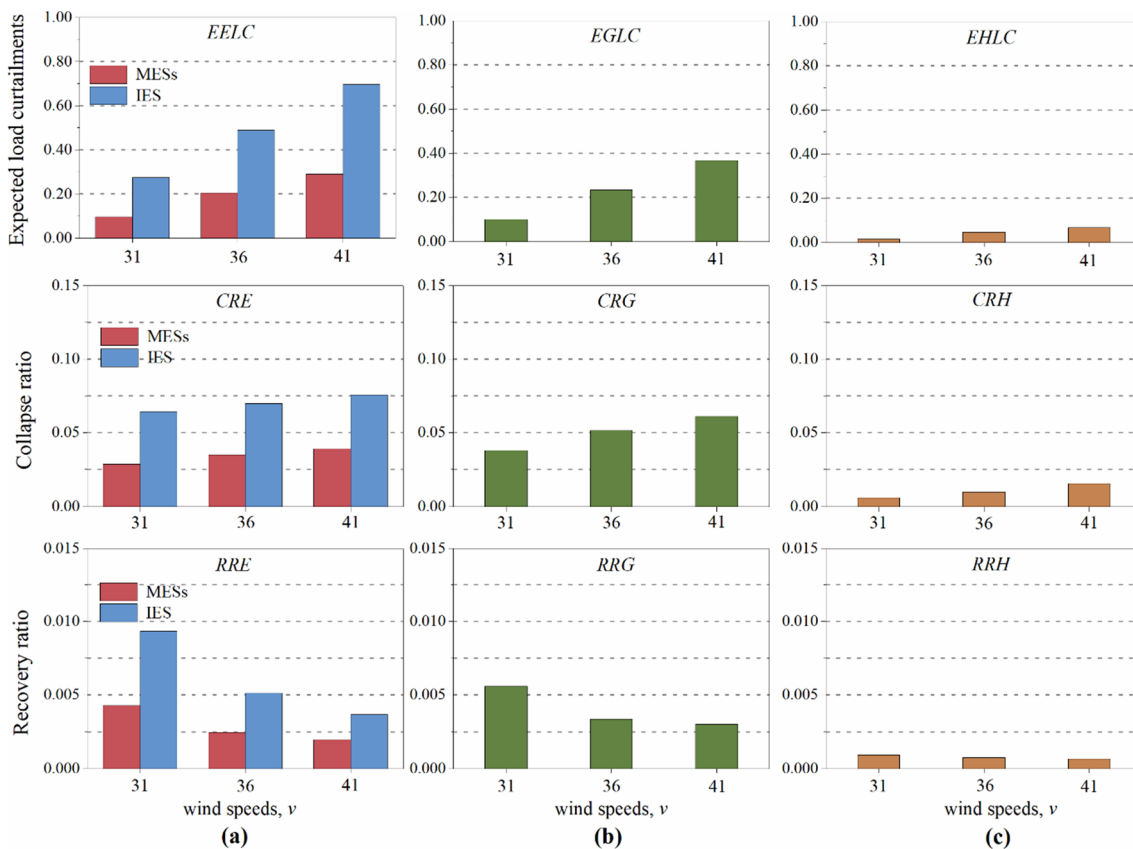


**Fig. 11.** Resilience metrics of MESs for different wind speeds. (a) Electric resilience metrics. (b) Gas resilience metrics. (c) Heat resilience metrics.

**Table 4**

Comparison of SEL between MESs and IESS for different wind speeds.

Test systems	$v = 31 \text{ m/s}$	$v = 36 \text{ m/s}$	$v = 41 \text{ m/s}$
MESs	0.0795	0.1750	0.2781
IES	0.0934	0.1667	0.2369

the resilience of MESs.

### 5.2.3. Case 3: Correlation analysis between resilience and economy

In the previous cases, the resilience of heat subsystems is improved at the cost increased investment, since gas boilers, heat pumps and CHP are introduced to supply heat. In order to show the correlation between resilience and cost, two scenarios are introduced with different components contained in EH. Scenario A is the base case with the largest cost, where the EH contains gas boilers, heat pumps and CHP. In scenario B, only the CHP is introduced in EH to supply heat. In accordance with case 1, the resilience of MESs in these two scenarios is evaluated under grid-scale windstorms with 31 m/s, 36 m/s and 41 m/s wind speeds. The techniques to determine the failure probability of components, the repair time TTR of damaged components and the duration of phase III are identical to those in case 1.

The resilience metrics of MESs are compared between two scenarios

**Table 5**

The computation time of resilience evaluation for different wind speeds.

Wind speeds	Average computation time of optimal energy flow model (s)	Average computation time per sample (s)	Total calculation time (s)
$v = 31 \text{ m/s}$	4.61	35.40	43152.60
$v = 36 \text{ m/s}$	4.67	49.33	66348.85
$v = 41 \text{ m/s}$	4.58	66.78	80336.34

**Table 6**

Illustration of four scenarios with different regional wind speeds.

Wind speeds (m/s)	Scenario A	Scenario B	Scenario C	Scenario D
$v_1$	41 m/s	20 m/s	20 m/s	41 m/s
$v_2$	20 m/s	41 m/s	20 m/s	31 m/s
$v_3$	20 m/s	20 m/s	41 m/s	20 m/s

for different wind speeds, as shown in Table 8. It can be noted that the values of EHLC in scenario B are much larger than those in scenario A, indicating that the removal of gas boilers and heat pumps in EH can significantly reduce the resilience of heat subsystems. The EHLC values in scenario B are 2.69, 5.76 and 6.01 times than those in scenario A for 31 m/s, 35 m/s and 41 m/s wind speeds, respectively. The findings reveal the inverse correlation between system resilience and cost. Moreover, the removal of elements in EH has little effects on the resilience of electric and gas systems, since the change of EELC and EGRC values are small from scenarios A to B. Furthermore, the values of EELC in scenario B are smaller than those of IES, whose resilience metrics are given in Fig. 10. The results show that the CHP units can significantly improve the resilience of power systems compared to gas boilers and heat pumps.

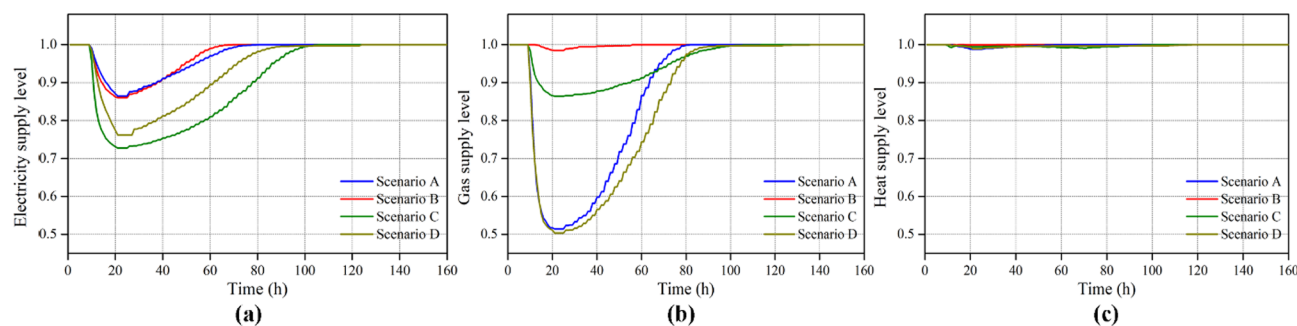


**Fig. 12.** Energy supply level of MESs as a function of time for different scenarios. (a) Electricity supply level. (b) Gas supply level. (c) Heat supply level.

**Table 7**  
System resilience metrics of MESs for different scenarios in case 2.

Energy carriers	Resilience metrics	Scenario A	Scenario B	Scenario C	Scenario D
Electricity	<i>EELC</i>	0.0391	0.0402	0.1163	0.0819
	<i>CRE</i>	0.0114	0.0115	0.0208	0.0202
	<i>RRE</i>	0.0018	0.0022	0.0027	0.0021
Gas	<i>EGLC</i>	0.1731	0.0024	0.0543	0.2009
	<i>CRG</i>	0.0369	0.0014	0.0109	0.0362
	<i>RRG</i>	0.0072	0.0002	0.0014	0.0046
Heat	<i>EHLC</i>	0.0023	0.0003	0.0036	0.0045
	<i>CRH</i>	0.0011	0.0002	0.0010	0.0010
	<i>RRH</i>	0.0002	0.0001	0.0002	0.0001

## 6. Conclusions

The growing frequency and extent of windstorm events entail the need to analyze the resilience of multi-energy systems (MESs). This paper proposes a comprehensive framework to evaluate the impacts of windstorms on the nodal resilience of MESs. The multi-phase performance response curve is utilized to characterize the time-dependent performance levels of MESs at different phases, where the impacts of weather extent on component and system operation are modeled. Moreover, a service-based optimal energy flow model is proposed to assess the performance losses of MESs under windstorms through the coordination among different energy subsystems. Furthermore, nodal resilience metrics for different energy subsystems are defined to quantitatively evaluate the resilience of MESs.

Case studies demonstrate that the increase of weather extent can dramatically decrease the system resilience indicators of MESs. Regarding the resilience of energy subsystems, the heat system can be more resilient than electric system and gas system since the heat demands are simultaneously supplied by electricity and gas through the energy hub (EH). Besides, due to the support of power supply from combined heat and power units of EH, the resilience of electric system in MESs can be highly improved compared to isolated electric systems.

**Table 8**  
System resilience metrics of MESs for different scenarios and wind speeds.

Resilience metrics	$v = 31 \text{ m/s}$		$v = 35 \text{ m/s}$		$v = 41 \text{ m/s}$	
	Scenario A	Scenario B	Scenario A	Scenario B	Scenario A	Scenario B
<i>EELC</i>	0.0960	0.0992	0.2040	0.2017	0.2895	0.2783
<i>EGLC</i>	0.0998	0.0933	0.2340	0.2342	0.3677	0.3420
<i>EHLC</i>	0.0061	0.0164	0.0102	0.0588	0.0159	0.0956

Under the impacts of region-scale windstorms, the values of resilience indicators of area 3 in MESs is the smallest among all areas. Therefore, it is an effective measure to harden electrical components in area 3 for improving the resilience of MESs. Moreover, the removal of gas boilers and heat pumps in EH can significantly reduce the resilience of heat subsystems, revealing the inverse correlation between system resilience and cost. The proposed model and method can provide system operators with a useful tool to analyze the resilience of MESs under windstorms. Furthermore, the previous findings can effectively guide system operators to constitute targeted measures to enhance the resilience of MESs.

In this study, it is assumed that the storms have constant wind speeds in one region without considering the varying weather conditions over time. When considering the temporal wind speeds, the failure probability of components can change with time, which is not considered in this study. Nevertheless, the multi-phase simulation framework in this paper can be applied to the resilience of MESs under varying weather conditions, if the time series of wind speeds are determined. In specific, the failure probability of electric components at different time steps can be calculated according to the time series of wind speeds using the failure models in (4)–(6). By sampling component failures using the Monte-Carlo simulation technique, the resilience of MESs under windstorms can be evaluated using the proposed multi-phase framework. Concerning the determination of time series of weather conditions, several methods can be utilized, including statistical analysis methods [38] and projection models [21]. In future work, the analysis framework in this paper can be expanded to evaluate the resilience of MESs under various weather conditions.

## CRediT authorship contribution statement

**Minglei Bao:** Conceptualization, Methodology, Software, Writing - original draft. **Yi Ding:** Writing - review & editing, Supervision. **Maosheng Sang:** Resources, Data curation. **Daqing Li:** Writing - review & editing. **Changzheng Shao:** Visualization, Validation. **Jinyue Yan:** Writing - review & editing.

## Declaration of Competing Interest

The authors declare that they have no known competing financial interests or personal relationships that could have appeared to influence the work reported in this paper.

## Acknowledgments

The research is supported by the China NSFC under Grant 71871200 and National Natural Science Foundation China and Joint Programming Initiative Urban Europe Call (NSFC-JPI UE) under grant 71961137004.

## Appendix A. The mathematical descriptions for piecewise linearization of pipeline flow

Corresponding to the pipeline flow in (16), the flow squared  $|f_{mn}^t| \cdot f_{mn}^t$  and pressures squared  $(\pi_m^t)^2$ ,  $(\pi_n^t)^2$  need to be linearized [33]. Firstly, new variables  $ps_m^t$  are introduced to replace the nodal pressures squared  $(\pi_m^t)^2$ , which can be expressed as:

$$ps_m^t = (\pi_m^t)^2 \quad (46)$$

Furthermore, the nonlinear function  $|f_{mn}^t| \cdot f_{mn}^t$  can be regarded as the general form  $h(x) = x \cdot |x|$  defined on an interval  $D = [A, B]$ , where  $x = f_{mn}^t$ . Regarding pipeline flow  $f_{mn}^t$ , the operating interval  $[A, B]$  can be determined by the transmission capacity of pipelines. By dividing the operating interval at the demarcation points  $A = X_1 \leq \dots \leq X_z \leq \dots \leq X_Z = B$  with corresponding function values  $h(X_z)$ , the non-linear function  $h(x) = x \cdot |x|$  can be separated into  $Z - 1$  linear segments, as shown in Fig. 13. On the basis, the method to approximate  $h(x)$  can be formulated as follows:

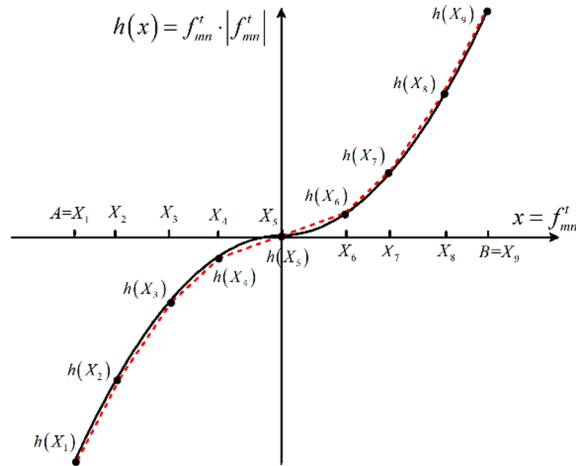


**Fig. 13.** Piecewise linearization of the pipeline flow squared.

$$h(x) \approx h(X_1) + \sum_{z=1}^{Z-1} [h(X_{z+1}) - h(X_z)] \delta_z \quad (47)$$

$$x = X_1 + \sum_{z=1}^{Z-1} (X_{z+1} - X_z) \delta_z \quad (48)$$

$$\delta_{z+1} \leq \sigma_z \leq \delta_z, \quad z \in \{1, \dots, Z-2\} \quad (49)$$

$$0 \leq \delta_z \leq 1, \quad z \in \{1, \dots, Z-1\} \quad (50)$$

where  $\delta_z$  denotes continuous variable representing the portion of pipeline flow.  $\sigma_z$  is binary variable to force that if an interval  $[X_{z-1}, X_z]$  is chosen, all intervals to its left must be completely used.

By applying the piecewise linearization techniques in (47)–(50), the pipeline flow function in (16) can be approximated as:

$$|LF_{mn,1}^t| \cdot LF_{mn,1}^t + \sum_{z=1}^{Z-1} (|LF_{mn,z+1}^t| \cdot LF_{mn,z+1}^t - |LF_{mn,z}^t| \cdot LF_{mn,z}^t) \delta_z = M_{mn} \cdot (ps_m^t - ps_n^t) \quad (51)$$

$$f_{mn}^t = LF_{mn,1}^t + \sum_{z=1}^{Z-1} (LF_{mn,z+1}^t - LF_{mn,z}^t) \quad (52)$$

$$\delta_{z+1} \leq \sigma_z \leq \delta_z, \quad z \in \{1, \dots, Z-2\} \quad (53)$$

$$0 \leq \delta_z \leq 1, \quad z \in \{1, \dots, Z-1\} \quad (54)$$

where  $LF_{mn,z}^t$  denotes  $z$ th segment for the gas flow of pipeline  $mn$  at time  $t$ .

## References

- [1] Jin X, Mu Y, Jia H, Wu J, Xu X, Yu X. Optimal day-ahead scheduling of integrated urban energy systems. *Appl Energy* 2016;180:1–13.
- [2] Gabrielli P, Gazzani M, Martelli E, Mazzotti M. Optimal design of multi-energy systems with seasonal storage. *Appl Energy* 2018;219:408–24.
- [3] Ma T, Wu J, Hao L, Lee W-J, Yan H, Li D. The optimal structure planning and energy management strategies of smart multi energy systems. *Energy*. 2018;160:122–41.
- [4] Panteli M, Mancarella P. Modeling and evaluating the resilience of critical electrical power infrastructure to extreme weather events. *IEEE Syst J* 2015;11:1733–42.
- [5] Abdin I, Fang Y-P, Zio E. A modeling and optimization framework for power systems design with operational flexibility and resilience against extreme heat waves and drought events. *Renew Sustain Energy Rev* 2019;112:706–19.
- [6] Lin Y, Bie Z. Study on the resilience of the integrated energy system. *Energy Procedia* 2016;103:171–6.
- [7] The Natural Gas Grid Needs Better Monitoring. [online]. <https://issues.org/the-natural-gas-grid-needs-better-monitoring/>.
- [8] Lu J, Guo J, Jian Z, Yang Y, Tang W. Resilience assessment and its enhancement in tackling adverse impact of ice disasters for power transmission systems. *Energies* 2018;11:2272.
- [9] Hosseini S, Barker K, Ramirez-Marquez JE. A review of definitions and measures of system resilience. *Reliab Eng Syst Saf* 2016;145:47–61.
- [10] Liu H, Davidson RA, Apanasovich TV. Statistical forecasting of electric power restoration times in hurricanes and ice storms. *IEEE Trans Power Syst* 2007;22:2270–9.
- [11] Nateghi R, Guikema SD, Quiring SM. Comparison and validation of statistical methods for predicting power outage durations in the event of hurricanes. *Risk Anal: Int J* 2011;31:1897–906.
- [12] Ouyang M, Dueñas-Osorio L, Min X. A three-stage resilience analysis framework for urban infrastructure systems. *Struct Saf* 2012;36:23–31.
- [13] Panteli M, Pickering C, Wilkinson S, Dawson R, Mancarella P. Power system resilience to extreme weather: fragility modeling, probabilistic impact assessment, and adaptation measures. *IEEE Trans Power Syst* 2016;32:3747–57.
- [14] Cadini F, Agliardi GL, Zio E. A modeling and simulation framework for the reliability/availability assessment of a power transmission grid subject to cascading failures under extreme weather conditions. *Appl Energy* 2017;185:267–79.
- [15] Cimellaro GP, Villa O, Bruneau M. Resilience-based design of natural gas distribution networks. *J Infrastruct Syst* 2014;21:05014005.
- [16] Panteli M, Mancarella P, Trakas DN, Kyriakides E, Hatziargyriou ND. Metrics and quantification of operational and infrastructure resilience in power systems. *IEEE Trans Power Syst* 2017;32:4732–42.
- [17] Ouyang M, Dueñas-Osorio L. Time-dependent resilience assessment and improvement of urban infrastructure systems. *Chaos: An Interdisciplinary J Nonlinear Sci* 2012;22:033122.
- [18] Ouyang M, Dueñas-Osorio L. Multi-dimensional hurricane resilience assessment of electric power systems. *Struct Saf* 2014;48:15–24.
- [19] Francis R, Bekera B. A metric and frameworks for resilience analysis of engineered and infrastructure systems. *Reliab Eng Syst Saf* 2014;121:90–103.
- [20] Bao M, Ding Y, Singh C, Shao C. A multi-state model for reliability assessment of integrated gas and power systems utilizing universal generating function techniques. *IEEE Trans Smart Grid* 2019;10:6271–83.
- [21] Zhang H, Cheng L, Yao S, Zhao T, Wang P. Spatial-temporal reliability and damage assessment of transmission networks under hurricanes. *IEEE Trans Smart Grid* 2019. <https://doi.org/10.1109/TSG.2019.2930013>.
- [22] Sheng W, Yi D, Chengjin Y, Can W, Yuchang M. Reliability evaluation of integrated electricity–gas system utilizing network equivalent and integrated optimal power flow techniques. *J Mod Power Syst Clean Energy* 2019;7:1523–35.
- [23] de Bruin W. Analyzing the value of energy hubs in multi-energy distribution systems Bachelor thesis Power Systems Laboratory, ETH Zurich; 2009
- [24] Khan MS, Chaniago YD, Getu M, Lee M. Energy saving opportunities in integrated NGL/LNG schemes exploiting: thermal-coupling common-utilities and process knowledge. *Chem Eng Process Process Intensif* 2014;82:54–64.
- [25] Morvaj B, Evins R, Carmeliet J. Optimization framework for distributed energy systems with integrated electrical grid constraints. *Appl Energy* 2016;171:296–313.
- [26] Ohshita S, Johnson K. Resilient urban energy: making city systems energy efficient, low carbon and resilient in a changing climate. European Council for an Energy Efficient Economy[online]. <https://www.eceee.org/library/conference-proceedings/eceee-Summer-Studies/2017/3-local-action/resilient-urban-energy-making-city-systems-energy-efficient-low-carbon-and-resilient-in-a-changing-climate>; 2017.
- [27] Mensah AF. Resilience assessment of electric grids and distributed wind generation under hurricane hazards; 2015.
- [28] Mehrtash A, Wang P, Goel L. Reliability evaluation of power systems considering restructuring and renewable generators. *IEEE Trans Power Syst* 2012;27:243–50.
- [29] Electricity Customers. [online]. <https://www.epa.gov/energy/electricity-customers>.
- [30] Use of natural gas. [online]. <https://www.eia.gov/energyexplained/natural-gas/use-of-natural-gas.php>.
- [31] Martinez-Mares A, Fuerte-Esquivel CR. A unified gas and power flow analysis in natural gas and electricity coupled networks. *IEEE Trans Power Syst* 2012;27:2156–66.
- [32] Jia H, Ding Y, Song Y, Singh C, Li M. Operating reliability evaluation of power systems considering flexible reserve provider in demand side. *IEEE Trans Smart Grid* 2018;10:3452–64.
- [33] Correa-Posada CM, Sanchez-Martin P. Integrated power and natural gas model for energy adequacy in short-term operation. *IEEE Trans Power Syst* 2014;30:3347–55.
- [34] Zhou Y, Gu C, Wu H, Song Y. An equivalent model of gas networks for dynamic analysis of gas-electricity systems. *IEEE Trans Power Syst* 2017;32:4255–64.
- [35] De Wolf D, Smeers Y. The gas transmission problem solved by an extension of the simplex algorithm. *Manage Sci* 2000;46:1454–65.
- [36] Chicco G, Mancarella P. Matrix modelling of small-scale trigeneration systems and application to operational optimization. *Energy* 2009;34:261–73.
- [37] Bao M, Ding Y, Shao C, Yang Y, Wang P. Nodal reliability evaluation of interdependent gas and power systems considering cascading effects. *IEEE Trans Smart Grid* 2020. <https://doi.org/10.1109/TSG.2020.2982562>.
- [38] Perera A, Nik VM, Chen D, Scartezzini J-L, Hong T. Quantifying the impacts of climate change and extreme climate events on energy systems. *Nature Energy* 2020;1:10.